University of Alberta

Improving the photostability of aramid fabric by sol-gel coating

by

Lidan Song

A thesis submitted to the Faculty of Graduate Studies and Research
in partial fulfillment of the requirements for the degree of

Master of Science
in
Textiles and clothing

Department of Human Ecology

Fall 2011
Edmonton, Alberta

ABSTRACT

Limited studies have shown effective ways to protect aramid fabrics from photodegradation. The purpose of this research is to find an effective and feasible method to improve the photostability of Nomex® aramid fabric. An inorganic titanium dioxide sol-gel is used as a UV-protective coating on the fabric surface. The effectiveness of the sol-gel coating in preventing photodegradation is determined by examining changes in mechanical properties, chemical composition, as well as surface morphology structure of the coating. Findings show that nano scale anatase titanium dioxide thin films were formed on the fabric surface and decreased the photodegradation rate of the Nomex® aramid fabric.

ACKNOWLEDGEMENTS

First and most, I will thank my supervisor Dr. Guowen Song, whose inspiring guidance and endless patience lead to the completion of this thesis.

Secondly, I wish to thank Dr. Jane Batcheller and Dr. Hongbo Zeng. Dr. Batcheller's assistance in the accelerated photodegradation experiments made the completion of this thesis possible. As her teaching assistant in the past years, I learned not only the knowledge but also a scientific attitude from her. Dr. Zeng's knowledge of material science enriched the content of this thesis. I also wish to express my appreciation to Dr. Rachel McQueen for her assistance in statistical analysis and interpretation and Dr. Nancy Kerr for her suggestions and patience in the thesis revision. Acknowledgement is also sent to Professor Jinbo Yao and Professor Jianfei Zhang at Tianjin Polytechnic University in China for their help in providing experiment equipment and setups.

I also want to express my gratitude to my friends. Their care and encouragement made my study in Edmonton and my life more colorful. They are Pipi, Shuqin, Tannie, Tianhong, Yin, Sihong, Dan, Linlin as well as Yanan.

Last, but not the least, I will thank my family, the most important people in my life. Their endless love and support gave me courage and determination to pursue my master's degree in Canada.

TABLE OF CONTENTS

LIST OF TABLES

LIST OF FIGURES

CHAPTER 1 INTRODUCTION

BACKGROUND

As the general concern regarding health and safety of workers under various circumstances becomes more significant, the importance of protective clothing has been well recognized in the textile industry and research. Protective clothing can provide a microenvironment where the human body is isolated from external dangers that may result in injuries or death. Protective clothing works as the last and nearest line of defense for the human body against external hazards, especially in extreme disasters and war conditions. For example, respirators and protective clothing played an important role in protecting the firefighters against the flame, dust and asbestos released from the collapse of the Twin Towers in the 9/11 attacks. It was reported that the majority of the first respondents who did not have such protection had a higher risk of suffering from mesothelioma, a kind of cancer linked directly to asbestos exposure (Mesolik org., 2009). In 2010, oil cleanup crew wore the white Tyvek® protective clothing while they were cleaning the oils after the April 20th well blowout accident in the Gulf of Mexico (Bourne, 2010) to avoid the contamination from oil dusts.

Protective clothing is widely used in industries, agriculture, military, sports, medicine, and some civilian activities. According to the end use functions, protective clothing can be classified into six general categories: thermal protective clothing, chemical protective clothing, mechanical protective clothing, radiation protective clothing, biological protective clothing, and electrical protective clothing (Zhou, Reddy, & Yang, 2005).

Thermal protective clothing protects the human body from thermal hazards such as fire, hot steam, and hot liquid. Heat normally transfers in three ways: conduction, convection, and radiation. To reduce the heat transfers from outer hazards to human body, thermal protective clothing is usually designed into multilayers - typically a three layer systems including shell fabric, moisture barrier and thermal liner (Davis, Chin, Lin, & Petit, 2010).

Chemical protective clothing is often used in chemical factories, chemical labs, agricultural activities and emergency circumstances where people may be required to handle dangerous or toxic chemicals. Usually the solubility and permeation of chemicals by clothing materials are used to evaluate the barrier effect of chemical protective clothing (Raheel, 1994). An important index is the breakthrough time of permeation. In order to meet the needs of different situations, chemical protective clothing is designed into fully encapsulating or non-encapsulating styles (Zhou *et al.*, 2005).

Mechanical protective clothing protects people from mechanical impact hazards. One example is the ballistic protective clothing used for soldiers, policemen, and security personnel. Jacobs and van Dingenen stated that the protective ability of ballistic protective clothing depended on how fast it absorbed the energy from impact object and transferred the energy (as cited in Zhou *et al.*, 2005). High performance fibres Kevlar® and Zylon® are usually applied in mechanical protective clothing as they have been proven to have good resistance to mechanical impacts.

Radiation protective clothing is mainly used to prevent the exposure of the human body to nuclear radiation, ultraviolet radiation and electromagnetic radiation

(Zhou *et al.*, 2005). Nuclear radiation may result in serious injury to human skin, eyes, nose and mouth. Weak radiation can be shielded by goggles, masks, gloves and protective clothing. However, short wave radiation can penetrate textiles. It is important to control the radiation contamination, exposure time and distance from the radiation source to the human body in Adanur's study (as cited in Zhou *et al.*, 2005). UV protection becomes critical as the skin cancer was reported to have increased in recent years (Hoffmann, Laperre, Avermaete, Altmeyer & Gambichler, 2001). UV protective clothing is designed to decrease the amount of UV radiation to skin surface as much as possible. The fibre type, fabric construction, fabric thickness and color may affect the effectiveness of UV protective clothing.

As the protective clothing plays an essential role in protecting human beings, protective clothing needs to meet various standards for safety and quality assurance. Various performance specifications exist to regulate the manufacture and evaluation of different categories of protective clothing. For example, Standard ASTM F1407 regulates a cup method to test the liquid permeation for chemical protective clothing (2006). Standard ASTM F1930 developed an instrumental manikin testing for flame resistance clothing (2008).

To meet the needs of various protective clothing, the textile fibres used for protective clothing require some specific properties. They usually have high tenacity, high modulus, chemical resistance, or thermal resistance. Fibres with these properties are often referred to as high performance fibers. In thermal protective clothing, multiple fabric systems including flame retardant viscose, flame resistant cotton and nonflammable aramid fabrics are used. In mechanical protective clothing, high strength, high energy absorbing fibres are employed.

High performance fibres were initially developed for use in military and aerospace applications. Their outstanding thermal, mechanical and chemical properties enabled them to be used in ground vehicles, aircrafts and soldier protection systems. In recent years, the global war against terrorism has increased the military usage of high performance fibres to protect crew (National research council, 2005). At the same time, as the cost of production has decreased and the market demand has increased, the applications for high performance fibres has now extended to commercial aircraft, civil construction, engineering, sports and recreation equipment (National research council, 2005).

This trend of increasing market demand drove the growth of the high performance fibre industry. The first commercial introduction of organic high performance fibre was the meta-aramid fibre Nomex® developed by DuPont in late 1960s (DuPont, 2001). Since then, the demand for high performance fibres has increased steadily. It was reported that the demand for meta-aramid and para-aramid fibres grew at a 6% to 7% rate from the later 1970s to the mid-1990s and these two fibre types totally contributed to more than 90% of the worldwide demand for high performance fibres (National research council, 2005). Therefore in 2004, DuPont announced a more than $70 million investment in its para-aramid Kevlar® production to meet the market demand (National research council, 2005).

High performance fibres are also used in protective clothing systems including helmets, soft armor, boots and respiratory equipment. For example, the para-aramid fibre, Kevlar® is made into ballistic armor because it is good at absorbing mechanical impact energy. The meta-aramid fibre, Nomex® is usually used in firefighter garments due to its excellent flame resistance. However, the durability of high performance fibres is now becoming a concern for protective

clothing. The drawback in their properties and the damages caused during service may impair the protective functions. For example, high performance fibres are usually very sensitive to ultraviolet radiation due to their unsaturated chemical structure. According to a recent study on structural fire fighter protective clothing, the outer shell that was made by polyaramid and polybenzimidazole were damaged by ultraviolet light radiation. The outer shell fabrics lost more than 40% of their tear resistance and tensile strength after 13 days of exposure to simulated ultraviolet light (Davis *et al.*, 2010).

STATEMENT OF PROBLEM AND PURPOSE

With excellent mechanical and chemical properties, aramid fibers are extensively used in protective clothing, building materials, sport equipment, etc. However, aramid fibers are vulnerable to UV radiation due to their unsaturated chemical structure. Photodegradation happens to aramid fibers during UV exposure and as a result, the mechanical properties decrease significantly. This property lowers the service life of aramid fiber products. The purpose of the thesis project is to develop an effective method to improve the photostability of aramid fabrics.

Existing research examines the photodegradation mechanism of high performance polymers and various methods to enhance the photostability of conventional apparel materials such as cotton and polyester (Xin, Daoud, & Kong, 2004; Awitor, Rivaton, Gardette, Down, & Johnson, 2008), but does not explore an effective method to protect aramid high performance materials from ultraviolet degradation. This study will address this gap by using a sol-gel surface coating method (Mahltig, Haufe, & Böttcher, 2005; Daoud & Xin, 2004) to create a titanium dioxide thin film on the surface of aramid fabric to improve its photostability.

A quantitative paradigm informs the design of this study, because the study follows a natural science model, where the observable variables give numerical data that are emphasized for their precision and amenability to mathematical analysis to test the hypotheses. In this study, physical properties and chemical composition of the fabric are tested on apparatus to get quantitative data before and after sol-gel coating to evaluate the effectiveness of the treatment.

JUSTIFICATION

The high performance properties of aramid fibre make it widely applicable in industries, agriculture, military, sports, medicine, and some civilian activities. It is also used in protective clothing. However, the unsaturated chemical structure of aramid fibre determines that it is vulnerable to photo radiation. The photo radiation damages the structure of aramid fibre leading to the failure of mechanical properties. As the sol-gel coating is widely reported to enhance the properties of textile materials (Mahltig *et al.*, 2005), it provides an approach to improve the photostability of aramid fibre. Due to the lack of research on this topic, it is unknown whether the sol-gel coating would work effectively to enhance the photostability of aramid fibre. This study explores the possibility to improve the photostability of aramid fibre using a sol-gel coating of titanium dioxide.

This study is a significant contribution to the research of photodegradation of high performance textile materials and sol-gel science. It also benefits textiles and clothing scholarship by exploring the artificial modification on high performance apparel materials to make up the property deficiency so that this deficiency would not restrict their further applications. Findings have showed remarkable improvement in the photostability of the aramid fabric, the changes of mechanical property and chemical structure of aramid fabric with the photo radiation time, the relationship between sol solution concentration and film thickness, the morphology and function of the film in blocking the photons from aramid fibre.

OBJECTIVE

The objective of this study is to:

(1) find an effective method to improve the photostability of aramid fabrics,

(2) investigate the effects of TiO_2 sol-gel coating on aramid fabrics in terms of mechanical properties, chemical composition and surface morphology.

NULL HYPOTHESES

To meet the second objective, the following null hypothesis was tested:

Null hypothesis: There is no significant difference between the photodegradation of the TiO_2 sol-gel coated aramid fabric and the photodegradation of the original uncoated fabric.

LIMITATIONS AND DELIMITATIONS

Limitations

The main limitation of this study was not being able to set technological conditions and parameters for the sol-gel coating on aramid fabric. Improving the photostability of aramid fabric by using a sol-gel coating method is a broad topic covering photochemistry of aramids, and sol-gel chemistry and sol-gel physics. This study only explored the feasibility of the proposal. The parameters used in this study were selected from relevant previous studies. Findings showed the relationship between the sol solution concentration and film thickness, and the relationship between film thickness and its effectiveness. However, they are only a small part of the whole topic. There still exist unsolved problems such as the effects of padding pressure, drying temperature and rate on the TiO_2 thin film.

Delimitations

Only greige aramid fabrics with specific weight and thickness were selected to receive the photodegradation experiments and sol-gel coating. The accelerated photodegradation experiment was set under specific conditions. It cannot fully represent actual service conditions. So caution should be taken when extending the conclusions from the accelerated photodegradation experiment to other conditions. The parameters of the accelerated photodegradation experiment should be reported when citing the conclusions.

DEFINITIONS

The following definitions are given in terms of the terminology in textiles and clothing and sol-gel science.

- *Aramid fibre* - a manufactured fibre in which the fibre-forming substance is a long chain synthetic polyamide in which at least 85% of the amide linkages are attached directly to two aromatic rings (Yang, 1993)
- *Aramid high performance fabric* - fabric woven from aramid yarns, which have high performance in mechanical, physical and chemical properties
- *Nomex*® - registered trademark for poly(*m*-phenylene isophthalamide)
- *Kevlar*® - registered trademark for poly(*p*-phenylene terephthalamide)
- *Zylon*® - registered trademark for poly(*p*-phenylene-2,6-benzobisoxazole)
- *Tyvek*® - registered trademark for flashspun high-density polyethylene fibre
- *Degradation* - a deleterious change in properties of a textile (Tubbs & Daniels, 1991)
- *Photodegradation* - degradation caused by the absorption of light or other radiation and by consequent chemical reactions (Tubbs & Daniels, 1991)
- *UV degradation* - degradation caused by radiant energy for which the wavelengths in the UV range of 100 - 400 nm
- *Greige* - descriptive of textile products before they are leached, dyed or finished (Tubbs & Daniels, 1991)
- *Unsaturated chemical structure* - a chemical structure that contains carbon-carbon double or triple bonds
- *Breaking strength* - the maximum tensile force observed during a test in which the specimen is stretched until it breaks (CAN/CGSB-4.2 NO.9.1-M90, 2004)

- *Artificial weathering* - exposure to cyclic laboratory conditions involving changes in temperature, relative humidity and radiant energy, with or without direct water spray, in an attempt to produce changes in the material similar to those observed after long-term, continuous, outdoor exposure (Tubbs & Daniels, 1991)
- *AATCC Fading Unit (AFU)* - a specific amount of exposure made under the conditions specified in various test methods where one AFU is one-twentieth (1/20) of the light-on exposure required to produce a color change equal to Step 4 on the Gray Scale for the Color Change or 1.7 ± 0.3 CIELAB units of color difference on AATCC Blue Wool Lightfastness Standard L4 (AATCC 16-2004, 2007)
- *Surface active agent* - an agent, soluble or dispersible in a liquid, which decreases the surface tension of the liquid (Klabunde & Richards, 2009)
- *Coated fabric* - a textile fabric on which there has been formed *in situ*, on one or both surfaces, a layer or layers of adherent coating materials (Tubbs & Daniels, 1991)
- *Sol* - a stable suspension of colloidal solid particles within a liquid (Brinker & Scherer, 1990)
- *Gel* - a porous 3-dimensionally interconnected solid network that expands in a stable fashion throughout a liquid medium (Brinker & Scherer, 1990)
- *Nano-sized particle* - particle sized between 1 and 100 nm (Klabunde & Richards, 2009)

CHAPTER 2 LITERATURE REVIEW

This chapter provides a review of aramid fibres, photodegradation of polymers, sol-gel coating and the practical methods used in photodegradation studies. The history, physical and chemical properties, and applications of aramid fibres give an overview of the aramid high performance material industry. Photodegradation of polymers introduces the basic photodegradation mechanism and the existing research in this field. Sol-gel coating explains how sol-gel science works and explores the possibility to apply a sol-gel coating to fibres. The practical methods part classifies the test and characterization approaches used in polymer photodegradation studies.

ARAMID HIGH PERFORMACE FIBRES

In the history of synthetic fibre, aromatic polyamide fibres appeared in 1960s and quickly became commercially available. The newly emerging fibres had excellent physical and chemical properties that enabled them to be widely used in industry and military applications. A word “aramid” was then invented to distinguish the aromatic polyamides from the conventional aliphatic polyamides nylon (Yang, 1989). In 1974, the United States Federal Trade Commission defined the term “aramid” as “a manufactured fibre in which the fibre-forming substance is a long chain synthetic polyamide in which at least 85% of the amide linkages are attached directly to two aromatic rings” (Yang, 1993, p.1).

Aramids are generated by the reaction between an amine group and a carboxylic acid halide group. The fibre molecular structure composed of the aromatic rings and the conjugated amide bonds is particularly strong. The crystallinity and

orientation of fibres are significantly improved as the polymer chains align regularly during the fibre manufacture process (Pegoretti & Traina, 2009). Aramid fibres offer excellent mechanical and chemical properties, thermal stability and flame resistance. Aramid fibres are also classified as high-tenacity, high-modules (HT-HM) fibers because of their outstanding tensile properties.

The first aramid fibre brand launched on the market is Nomex® for poly(*m*-phenylene isophthalamide) by DuPont in 1967 (DuPont, 2001). The original purpose of developing Nomex® fibre was to find an alternative fibre that would improve the thermal resistance of nylon. Kevlar®, poly(*p*-phenylene terephthalamide), is an isomer of Nomex®. Kevlar® fibre was introduced by DuPont in 1972. Until now, the aramid family encompasses commercial brands including Nomex®, Kevlar®, Teijinconex®, Technora®, and Twaron®.

Poly(m-phenylene isophthalamide) fibre

Poly(*m*-phenylene isophthalamide) fibre is a meta-aramid fibre. It is manufactured by a homogeneous dissolution polymerization process from two bifunctional aromatic organic compounds with groups in meta positions (Figure 1). After the polymerization process, a highly viscous solution with an average molecular weight of 100,000 is formed. The molecular weight distribution is determined by the type of polymerization, reactor, and reaction conditions (Horta, Coca, & Díez, 2003).

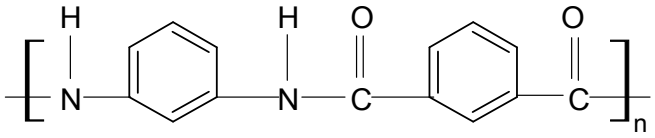

Figure 1. Chemical structure of poly(*m*-phenylene isophthalamide) fibre

The aromatic rings and the conjugated amide bonds primarily contribute to the excellent chemical and heat resistance. Nomex® fibre is inherently flame resistant. This high performance property does not diminish during the life of the fibre. The inherent non-flammability is due to the aromatic structure including high carbon to hydrogen ratio and high content of aromatic double bonds (Bourbigot & Flambard, 2002). The conjugation between the amide group and the aromatic ring increases the chain rigidity of Nomex® fibre (Gabara, Hartzler, Lee, Rodini, & Yang, 2006). The chain rigidity and hydrogen bonds restrain the movement of the polymer chains even under high temperature. When Nomex® fibre is approached to flame, it does not melt and drip and merely chars. When a Nomex® fabric is exposed to a flame, it hardens, starts to shrink, discolors, and chars thereby forming a protective coating. The Limited Oxygen Index (LOI) is usually used to evaluate the flammability of fabrics. Generally, a fabric with a LOI greater than 21% (the percent of oxygen in air) is self extinguished when removed from the flame source. The LOI of dyed Nomex® is 25%-27% while the LOI of natural Nomex® can be up to 28% (Carlsson & Wiles, 1973). Although it was found that the LOI of Nomex® was 30% to 32% (Afshari, Sikkema, Lee, & Bogle, 2008).

Nomex® 430 fibre has a 0.44 N/tex tensile strength, 30.5% elongation and an 8.32 N/tex initial modulus. Nomex® 450 fibre has a 0.26 N/tex tensile strength and a 22% elongation (Dupont, 2001). Nomex® fibres are widely used in thermal protective clothing because of the excellent flame resistance. It was reported that the Nomex® coveralls could provide protection for up to 17 seconds against an enveloping gasoline fire (Carlsson & Wiles, 1973). This is a significant time period for saving lives in real fire fighting. Nomex® are made into various kinds of firefighter garments and accessories. It is often used as a shell fabric to protect the thermal liner from further thermal damage in a multiple layer protective

systems. Nomex® are also widely made into thermal resistance furnishings, floor covering, and wall covering for schools and upholsters for cars and planes.

Poly(p-phenylene terephthalamide) fibre

Poly(*p*-phenylene terephthalamide) is an isomer of poly(*m*-phenylene isophthalamide). It is a para-oriented aramid fibre. Dupont launched the brand Kevlar® for poly(*p*-phenylene terephthalamide) fibre in 1972. The chemical structure of poly(*p*-phenylene terephthalamide) fibre is showed in Figure 2.

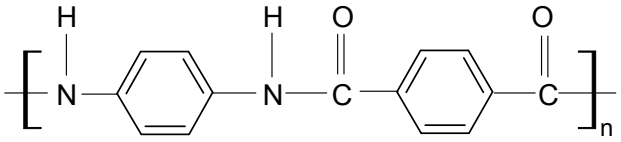

Figure 2. Chemical structure of poly(*p*-phenylene terephthalamide) fibre

The para-directed groups attached to the benzene rings in para-aramid fibre give it a rigid rod structure. Due to the insolubility of the rigid chain macromolecules, liquid crystalline spinning is applied (Rebouillat, 2001). During the spinning process the polymer chains' rod-like structures aggregate into ordered clumps running parallel to the flow. While passing through the spinneret the liquid-crystalline solution remains highly oriented creating highly crystalline fibres with excellent strength in the longitudinal direction (Afshari *et al.*, 2008). Kevlar® fibres have a skin-core structure, where the skin layer has a higher molecular orientation along the fibre axis determining a higher tenacity than the core of the fibre. In contrast to the zigzag meta-type structure of Nomex® fibres, Kevlar® fibres have a linear para-type structure.

Commercial Kevlar® fibre products include several major grades of filament

yarns such as high modulus yarn Kevlar® 49, high elongation yarn Kevlar® 119, high tenacity yarn Kevlar® 129, and ultra-high modulus yarn Kevlar® 149. The tensile trength of Kevlar® 49 is 2.04 N/tex with the initial modulus is 84.1 N/tex while the initial modulus of Kevlar® 149 can be up to 97.3 N/tex (Yang, 1993). The stress-strain curve shows that Kevlar® yarn has a breaking strength of 22-23 gpd which is about five times higher than that of steel wire (Yang, 1993) and four times than Nomex® fibre. In addition, Kevlar® fibres also offer excellent thermal stability under 500°C. They start to degrade severely when the temperature is higher than 500°C but they do not melt. Kevlar® fibres exhibit high flame retardancy with high limited oxygen index (LOI), low rate of heat release (RHR) and low smoke compared with natural fibres or other common synthetic fibres (Bourbigot & Flambard, 2002).

Para-aramids are widely used for ship building, pressure vessels, sports goods as well as protective clothing due to its light weight, high strength, high modulus, good impact strength, and wear resistance (Afshari *et al.*, 2008). For example, Nomex® fibres are used in fire fighter garments due to their good resistance to flame while Kevlar® fibres are used in ballistic body armor due to their excellent dynamic energy absorption.

Table 1. Property specifications of Nomex® and Kevlar® fibres (Afshari *et al.*, 2008)

Properties	Nomex®	Kevlar®
Density (g/cm^3)	1.38	1.45
Tensile strength (GPa)	0.65	3.6-4.1
Tensile modulus (GPa)	17	130-185
Decomposition temperature (°C)	400	550
LOI(%)	30-32	28-30

PHOTDEGRADATION OF POLYMERS

Polymer degradation happens commonly in the process of polymer manufacture, transportation, usage and conservation. According to the nature of the agents causing polymer degradation, the degradation can be classified into photodegradation, thermal degradation, ozone-induced degradation, mechanochemical degradation, catalytic degradation and biodegradation (Feldman, 2002; Singh & Sharma, 2008). Since more and more synthetic polymers are used in human lives, the polymer degradations are drawing much attention from polymer scientists. On one hand, to find effective methods to prevent degradations will improve the service lifetime of polymer products. On the other hand, to obtain powerful approaches to enhance degradations of disposal polymer products will have significant implication to environmental sustainability (Kaczmarek, Kamińska, Kowalonek & Szalla, 2000).

Mechanism of polymer photodegradation

Polymer photodegradation is caused by the absorption of energy from radiation. Absorbed energy breaks the bonds in polymers and causes subsequent chemical transformations. The general mechanism of photodegradation can be classified into three steps: Initiation, propagation and termination.

Initiation :	Initiator ($h\nu$)	⟶	$R_i\bullet$
	$R_i\bullet + O_2$	⟶	$R_iOO\bullet$
	$R_iOO\bullet + RH$	⟶	$R_iOOH + R\bullet$
Propagation :	$R\bullet + O_2$	⟶	$ROO\bullet$
	$ROO\bullet + RH$	⟶	$ROOH + R\bullet$
Termination :	$R\bullet + R\bullet$	⟶	R−R
	$R\bullet + ROO\bullet$	⟶	ROOR

Figure 3. Mechanism of polymer photodegradation (Singh & Sharma, 2008)

Initiation is the step where the radical is created by the absorption of sufficient radiation energy and the breaking of chemical bonds in polymer chains (Singh & Sharma, 2008). Yang (1993) summarized that two conditions must be fulfilled before the radiation of a given wavelength can cause the degradation of polymer fibers: wave absorption by the polymer and sufficient energy to break the chemical bonds. In order to activate the material molecules, enough radiation energy should be absorbed first.

Light exhibits the characteristic properties of both waves and particles. The particle of electromagnetic radiation is called a photon. The energy of a photon is calculated as:

$$\Delta E = h\nu \qquad \text{Eq (1)}$$

where E =Energy of a photon, h =Planck's constant (6.63×10^{-34} J•s),

ν = Frequency of the radiation, inversely related to the wavelength.

The energy of the radiation is related to the frequency, or inversely related to the wavelength of the radiation. Activation spectrum is usually used to show the effect of wavelength on the extent of degradation.

The Grotthus-Draper law states "only radiation that is absorbed by a substance may cause a chemical reaction" (Feller, 1994, p.45). Polymers having specific chromophoric groups in the chain tend to absorb the radiation energy that the radiation wavelength is in tune with the electronic system of the chromophoric group. The molecule is activated by the absorbed energy. Then the molecule will lose the energy

" a) by heat,

b) by the emission of radiation energy in form of fluorescence or phosphorescence,

c) by undergoing a chemical change within the molecule,

d) by the breaking of chemical bonds,

e) by transfer of the energy to another atom or molecule ” (Feller, 1994, p.49).

For different polymers, the mechanism involved in initiation is different under varied conditions. It can be summarized into six ways (Singh & Sharma, 2008):

a) direct UV initiated photolysis of C−C and C−H bond,

b) photosensitized cleavage,

c) catalyst residues as source of generation of radicals,

d) incorporation of carbonyl groups,

e) introduction of peroxides or site of unsaturation,

f) reactions of singlet and triplet stage.

The Stark-Einstein Law, also known as the law of photochemical equivalence, states that one atom or molecule is activated for every photon that is absorbed. Photochemists employed the concept of quantum yield or quantum efficiency to study the details of photochemical reactions for a given number of absorbed photons. Quantum yield is expressed as the number of molecules that is charged or decomposed for every photon of light absorbed. In the study of aramids photodegradation, Carlsson, Gan & Wiles (1978a & 1978b) used the quantum yields to compare the differences in aramid photodegradation between the absence of oxygen and presence of air. The quantum yields of aramid film samples irradiated in the absence of oxygen was less than 10^{-6} mole/einstein (Carlsson *et al*., 1978a) while the quantum yields in air was on the scale of 10^{-5}

mole/einstein (Carlsson *et al*., 1978b).

Propagation is the reaction of the carbon backbone with oxygen. Hydroperoxide species are generated in the process. Propagation normally includes two steps. The first step is the formation of polymer peroxy radicals (ROO•) by the reaction of polymer alkyl radicals (R•) with oxygen (O_2). The second step is the generation of a new polymer alkyl radical (R•) and polymer hydroperoxide (ROOH) by the abstraction of a hydrogen atom from the polymer peroxy radials (ROO•) (Rabek, 1990).

Termination is the step of the free radicals combining together, where the photodegradation reaction ends. Termination occurs both between two bimolecular radicals and also between low molecular radicals such as hydroxyl and hydroperoxy and other available radicals (Rabek, 1990). Rabek (1990) summarized the factors that may influence the termination reactions as:

"a) concentration of radicals formed;
b) effect of steric control and radical mobility in a polymer matrix;
c) cage effect;
d) mutual diffusion of reacting radicals;
e) structural parameters of the polymer matrix;
f) molecular-dynamical parameters of the polymer matrix;
g) light irradiation"(p.29).

In contrast to other degradations, photodegradation happens only on the substance surface. A thin surface layer only about 1μm degraded of a Nomex® film after 160 hours of radiation (Blais, Carlsson, Parnell & Wiles, 1973). The depth of visible and ultraviolet radiation that can penetrate into transparent or translucent

materials is related to the absorption coefficient of the medium and the radiation wavelength (Feller, 1994). Polymers exposed to light undergo chemical and physical changes which appear as the yellowing, embrittlement or loss in tensile strength.

Polymers can be grouped into highly photostable, moderately photostable and poorly photostable according to their photostability (Feldman, 2002). The factors that influence the photodegradation can be divided into two groups: the polymer factors and the ambient factors. The polymer factors such as polymer morphology and impurities play important roles in polymer photodegradation. For semicrystalline polymers, photo oxidation generally happens in amorphous regions causing the cleavage of polymer molecules and increase of the crystalline in polymer (Rabek, 1990). This was confirmed by the study of photodegradation of polyethylene (Torikai, Shirakawa, Nagaya & Fueki, 1990). The crystalline region in polymer is condensed and impermeable. The generated radicals in crystalline region cannot move as freely as those in amorphous regions. Moreover, oxygen cannot enter the crystalline region due to its impermeability. Thus, the photo oxidation is more prone to happen in amorphous regions. The short polymer chains caused by photo oxidation in amorphous regions pack together into an orderly fashion to increase the crystallinity of polymer (Rabek, 1990).

The environmental factors, including radiation intensity, radiation wavelength, temperature, humidity and the absence of oxygen, influence the polymer degradation (Gijsman, Meijers, & Vitarelli, 1999). The photo oxidation rate of polyethylene was linearly proportional to UV intensity (Jin, Christensen, Egerton, Lawson, & White, 2006). The rate also showed an increase with increasing

humidity and the oxygen content of the atmosphere (Jin *et al.*, 2006). The temperature would influence the degradation kinetic by affecting the mobility of free radicals (Rabek, 1990). Under high temperature, thermal degradation of polymer occurs simultaneously, which would enhance the photodegradation.

Various methods are applied in the degradation stimulations to study the polymer photodegradation. The natural weathering method is to expose the samples to full radiation spectrum outdoors. The altitude, temperature and humidity of the location influence the weathering results. This weathering process may last several months or even years. Rajakumar *et al* (2009) studied the natural weathering of polypropylene. Polypropylene films mounted on specially designed glass racks were directly exposed to solar radiation at the angle of 45° facing south at latitude 9.36°N and longitude 77.58°E. In total, the radiation lasted 6 months in both summer and winter seasons. The weathering parameters were recorded including the temperature, atmospheric pressure, UV and light intensity, humidity and rainfall (Rajakumar *et al.*, 2009). Among these natural parameters, temperature, UV and light intensity affected the degradation of the polypropylene films more than the other parameters. It was also concluded that the summer season generated a faster degradation of the films than the winter season did (Rajakumar *et al.*, 2009). However, due to the unpredictability and irreproducibility of the natural weather conditions, data from the natural weathering method are incomparable (Pospíšil *et al.*, 2006). Hence, an accelerated weathering method is usually used in laboratory tests by applying environmental chamber and artificial light source to simulate the natural conditions. It greatly reduced the test time and the weathering conditions can be controlled to a certain degree. Factors that affecting accelerated testing of polymer photostability were studied by Pospíšil *et al* (2006). The artificial light resources used in accelerated

weathering methods include mercury lamps with different pressure, xenon lamps, sodium lamps, tungsten lamps, vacuum ultraviolet sources, laser sources, etc (Rånby & Rabek, 1975). The light spectrum provided by different light sources is different and the light spectrum may vary in intensity with the temperature obtained in the lamp. The correlation between natural weathering and accelerated weathering was studied by Yang and Ding (2006). Polypropylene filaments were exposed to both solar radiation and UV fluorescent lamps with different intensity. The results showed that the lower intensities of UV radiation in accelerated weathering correlated well with natural weathering (Yang & Ding, 2006). Intensive accelerated weathering may cause "over-acceleration" (Pospíšil *et al*., 2006, p.418) which leads to bias in the results.

The photodegradation of aramid fibres

The unsaturated aromatic ring structures of aramid fibres, which have a greater potential for absorbing ultraviolet and visible radiation, make them susceptible to photo radiation. Carlsson *et al* (1978a & 1978b) studied the photodegradation mechanism of Nomex® fibres, in the absence of oxygen and in air respectively.

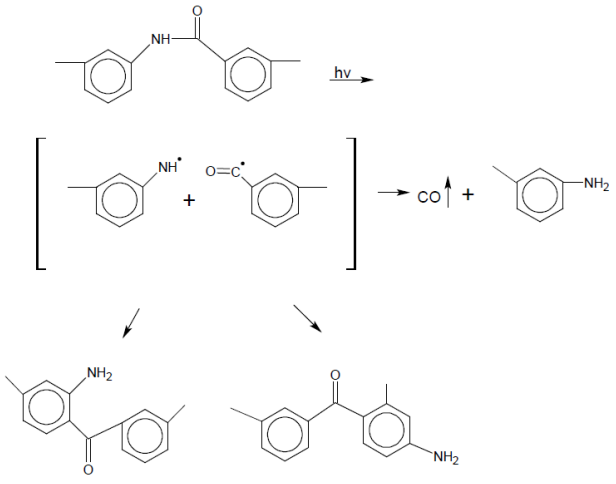

Figure 4. Photodegradation of Nomex® fibre in vacuum (Carlsson *et al.*, 1978a)

In a vacuum environment, Nomex® fibre photolysis reaction caused by ultraviolet radiation led to a photo-Fries rearrangement along the backbone (Figure 4). Photo-Fries rearrangement is an irradiation reaction of phenyl ester to produce both ortho and para rearrangement products and phenol (Kalmus & Hercules, 1972). The −CO−NH− bonds in the backbone were broken by the radiation energy then generated $-NH_2$ end groups and 2-aminobenzophenone units by evolution of CO (Carlsson *et al*., 1978a).

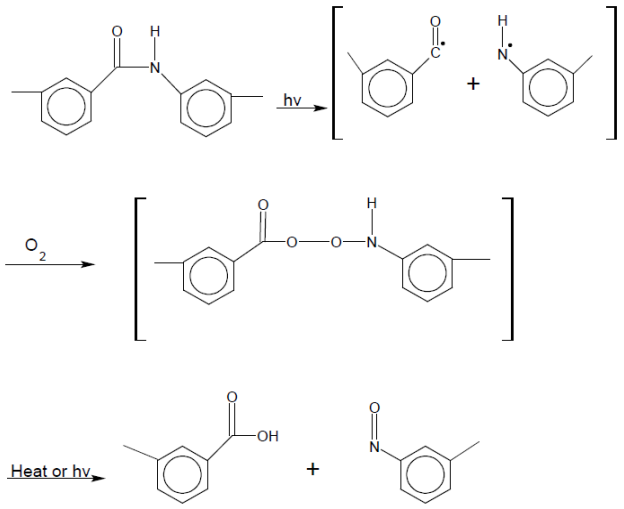

Figure 5. Photodegradation of Nomex® fibre in air (Carlsson *et al.*, 1978b)

In the presence of oxygen, the breaking −CO−NH− bonds reacted with the oxygen and formed −COOH and −N=O end groups (Figure 5).

The photochemical changes of three high performance fibres: Nomex®, Kynol®, and polybenzimidazole (PBI) were studied by X-ray photoelectron spectroscopy (XPS) (Hamilton, Sherwood, & Reagan, 1993). Fibre specimens were exposed to the filtered xenon lamp in an Atlas xenon weather-ometer at 63 ± 1°C and 65 ± 5% relative humidity (RH) for 160, 320, and 640 AATCC Fading Units (AFU),

respectively. To all of the specimens, the XPS spectra showed an increase of the O 1*s*/C 1*s* intensity ratio with the increase of the exposed time, which indicated the breakage of the C−C backbone of polymer and the oxidation of chemical groups. For Nomex® fibres, C 1*s* spectra indicated the formation of acid end groups as a result of the cleavage of amide linkages. The more rapid increase of O/C ratio of Nomex® compared to that of Kynol® and PBI fibre indicated Nomex® fibre was the most vulnerable fibre among them (Hamilton *et al*., 1993).

Exposure of unprotected Kevlar® yarns to ultraviolet light caused the loss of mechanical properties. After five months of outdoor exposure to the ultraviolet light, the tensile strength of Kevlar® yarns only retained 40% (Yang, 1993). The susceptibility of Kevlar® 49 fabrics woven in the UK and United States to photodegradation were investigated (Brown, Browne, Burchill & Egglestone, 1983). The warp and weft yarns of each fabric showed different susceptibility to the radiation-induced strength loss. The warp yarns of the UK fabric degraded faster than the weft yarns, and the reverse happened to the United States fabric. The authors figured out that the possible causes of this difference were the photosensitization of a surface active agent, the difference of the yarn diameters, and the molecular chain scission reactions (Brown *et al.*, 1983).

Zhang *et al* (2006) investigated the effects of UV irradiation on the mechanical and structural properties of Twaron® 2000, which was a kind of para-aramid fibre similar to Kevlar® 129. Twaron® 2000 fibre was exposed to a UV beam of wavelength ranging from 350 nm to 420 nm emitted by a carbon arc lamp at 40°C and 45% RH. The tensile data showed that the modulus, tenacity and work to break of the Twaron® 2000 fibre decreased quickly and almost linearly with the increasing of irradiation time. The UV beam etched the surface of the fibre and a

rougher surface image was shown by scanning electron microscopy after the irradiation. (Zhang *et al.*, 2006).

Photodegradation of structural firefighter protective clothing shell fabrics: NKB made of 93% poly(*m*-phenylene isophthalate), 5% poly(*p*-phenylene terephthalamide) and 2% antistatic fibres and KPB made of 60% poly(*p*-phenylene terephthalamide) and 40% polybenzimidazole fibres were studied by accelerated weathering (Davis *et al.*, 2010). The accelerated weathering was carried out at 50°C and 50% RH, which is close to the environment in which firefighter protective clothing is used. All fabrics showed a significant deterioration in the mechanical performance after exposure. However, the KPB fabric had a better resistance to the exposure than the NKB fabric by retaining a higher tensile strength and tear strength. Surface pitting and intersecting surface channels were observed on poly(*m*-phenylene isophthalate), poly(*p*-phenylene terephthalamide) and polybenzimidazole fibres. FTIR spectra showed that the proprietary polymeric water repellant coating on both fabrics was degraded after 13 days of radiation for KPB and 55 days of radiation for NKB. The Amide I and Amide II peaks had an intensity reduction after exposure indicating that the radiation energy broke the amide bonds in the polymer backbone. New peaks appeared with the formation of acids, alcohols and/or amines. Although UV radiation impaired the mechanical properties, and surface morphology and changed the chemical composition of the fibres, the fabrics still maintained a high level UV protection factor. Thus, the shell fabrics provided an excellent protection to undergarments from UV radiation.

Photostabilizers

The main function of photostabilizers is to inhibit or retard the rate of the

photodegradation reactions in polymers. A photostabilizer should be effective over a long period, should be distributed in the polymer matrix or on the surface of the polymer and be compatible with the polymer (Rabek, 1990). Photostabilizers are generally classified into four categories according to their ability (Rabek, 1990):

a) Screeners and absorbers: reduce the number of the photons absorbed by internal and external chromophores present in a polymer by reflecting, scattering or absorbing
b) Quenchers: deactivate excited states of chromophoric groups present in a polymer,
c) Decomposers: decompose hydroperoxide groups before they are photolysed by absorbed photons,
d) Free-radical scavengers: react with free radicals and thus interrupt degradative chain process.

Various types of photostabilizers have been already used in industry and research. Inorganic pigments such as iron oxides, chromic oxide, red lead oxide, zinc oxide, and titanium dioxide are widely used (Rånby & Rabek, 1975). Cotton fabrics treated with ZnO nanorods showed an excellent UV protection factor (Wang, Xin, Tao, & Daoud, 2004). ZnO particle-embedded acrylic coatings greatly prevented the ultraviolet degradation of Kevlar® fabric (Katangur, Patra & Warner, 2006). Al_2O_3, SiO_2, and ZnO had positive effects on the photo stabilization of linear low-density polyethylene respectively; however, the combination of either two agents had a negative effect (Yang, Li, &Yu, 2005).

Nanosized TiO_2 coating has effectively protected the aramid fibres from photodegradation (Xing & Ding, 2007; Li, Xing, & Ding, 2007). The working

mechanism of TiO_2 as a photostabilizer is still controversial. The photostabilizing ability of TiO_2 may be from its high refractive index by reflecting or scattering the UV rays or may be from its semiconductive properties by absorbing UV rays (Yang, Zhu, & Pan, 2004). TiO_2 is also reported to work as a photo catalyst to enhance the natural decomposition of polymers in the environment (Pandey, Kim, Chun, Lee, & Ahn, 2009) or to remove the impurities from water (Wold, 1993). In the photocatalytic reaction, TiO_2 absorbs UV radiation under 380 nm then generates electrons (e^-) and holes (h^+). With the presence of atmospheric oxygen, the electrons turn into reactive oxygen species superoxide radical anions (O_2^-); while the holes react with atmospheric water to generate hydroxyl radicals (•OH) and hydrogen peroxide (H_2O_2) (Zhang, Millington, & Wang, 2009). In the photostabilizing reaction, the working mechanism is explained by solid band theory (Yang *et al.*, 2004). The electrons (e^-) and holes (h^+) combine with other electrons or holes rather than react with atmospheric agents to generate superoxide products (Yang *et al.*, 2004). Among the different TiO_2 crystal forms, rutile was reported more suitable to be used as photostabilizer because of its high electron-hole recombination probability (Yang *et al.*, 2004). It is also demonstrated that nanoscale TiO_2 particles exhibit better UV-blocking capacity than that of the pigment scale TiO_2 particles (Yang *et al.*, 2004).

Organic photostabilizers include azo, quinoacridones, isoindolinones, perylenes, dioxazines and phthalocyanines, etc. Organic ultraviolet absorbers have been studied for both their interactions with other additives (Dobashi, Yuyama, & Ohkatsu, 2007) and the dependence of their performance on ultraviolet wavelength (Dobashi & Ohkatsu, 2008). Organic ultraviolet absorbers were classified as a hydrogen transfer type and a charge separation type (Dobashi *et al.*, 2007). Their performance in lowering the UV radiation reaction of substrate

correlated more with their maximum absorption wavelength than the molar extinction coefficient (Dobashi & Ohkatsu, 2008). It was also found that the combined use of two hydrogen transfer type ultraviolet absorbers would have a weaker synergism than the independent use while the mixture of a hydrogen transfer type ultraviolet absorber and a charge separation type ultraviolet absorber showed a strong synergism (Dobashi *et al.*, 2007).

In the study of the photodegradation of poly(ethylene terephthalate) (PET) films, ultraviolet stabilizers, including an organic ultraviolet absorber, carbon black and a mixture of TiO_2 and $BaSO_4$, were used to prevent weathering (Fechine, Rabello & Souto-Maior, 2002). A special weathering cycle was designed: 4 hours under UV light at 60°C and 4 hours in the dark under condensed water at 50°C. The organic ultraviolet absorber provided the most effective protection by retaining a lower carboxyl index and relatively higher tensile strength (Fechine *et al.*, 2002).

SOL-GEL COATING

Textile modification is an effective approach to improve textile properties. The modification methods are generally classified into three types: incorporation, grafting and coating (Mahltig, Haufe, & Böttcher, 2005). Incorporation is to add functional additives into the polymer melt or solution before spinning. Grafting is to link the functional additives on the surface of fibres by chemical reaction. Coating is to apply a thin film on the surface of fibres or fabrics. A coated fabric is defined as "a textile fabric on which there has been formed *in situ*, on one or both surfaces, a layer or layers of adherent coating materials" (Tubbs & Daniels, 1991, p.61). The gaps between the individual yarns are covered to varying degrees in fabric coatings. The earliest coating materials people used were natural

materials such as beewax, tars and gums (Fung, 2002). Coatings on modern textiles mainly contribute to the protection against wind, rain, chemicals, biological agents, microbes, etc.

Basic theory of sol-gel science

Sol-gel coating is a coating process based on sol-gel science. In contrast to conventional coating processes such as evaporation and sputtering, sol-gel coating can be done at room temperature and normal atmospheric pressure environment. Sol-gel coating is widely used to create a transparent metal oxide film that adheres well to the fibre surface to improve the textile properties such as abrasion resistance, electrical conductivity, UV protection, biocompatible properties and so on (Mahltig *et al.*, 2005).

A sol is "a stable suspension of colloidal solid particles within a liquid" (Brinker & Scherer, 1990, p.2). A gel is "a porous 3-dimensionally interconnected solid network that expands in a stable fashion throughout a liquid medium and is only limited by the size of the container" (Brinker & Scherer, 1990, p.8). The precursors of sols are usually two types: metallic salts and metal alkoxides. The choice of the solvent is either water or an organic liquid such as the corresponding parent alcohol (Brinker & Scherer, 1990). The solution chemistry of sols includes hydrolysis and condensation of precursors. The characteristic of particulate sols depends on the particle size, temperature and pH of the solution. The size of the particles must be small enough so that the repulsive force between the particles is greater than the force of gravity for the particles to stably exist in the liquid (Brinker & Scherer, 1990). The sol with particles smaller than 50 nm in diameter is also called a nanosol. The particle size tends to grow when the temperature increases as the higher temperature promotes the frequency of collisions and the

interactions leading to form clusters and aggregates. In Yu *et al*'s (2005) study, the preparation of nanosized TiO_2 from the hydrolysis of titanium *n*-butoxide was performed in an ice bath. The particle size is also pH dependent. Stable and clear sol with nanosized titanium dioxide can be obtained when pH < 3 or pH > 9 (Su, Hong & Tseng, 2004). In the sol-gel coating of silica thin film, lowering the pH and increasing the salt concentration led to larger size silica particles (Guleryuz, Kaus, Filiàtre, Grande, & Einarsrud, 2010).

The sol-gel coating process starts from the preparation of the sol solution by the corresponding precursor, and is then followed by the deposition of the sol to form a gel on the substrate. Finally a dense film is available by solvent evaporation and film condensation. The microstructure of the deposited film, i.e., the pore volume, pore size and surface area, can be controlled in the coating process. One factor is the size and extent of branching of the solution precursors. The other one is the evaporation and condensation during the deposition process (Brinker & Scherer, 1990). The evaporation of solvent compacts the film while the condensation stiffens the film to increase its resistance to compaction. The relative rates of condensation and evaporation determine the final microstructure of the film.

Applications

The advantages of sol-gel coating method made it widely used. It has a low requirement to the operating environment and is easy to control the film structure. Sol-gel coating was used on cotton fabrics to improve the ultraviolet protection factor (UPF) (Abidi, Hequet, Tarimala, & Dai, 2007), the hydrophobic property (Xue *et al.*, 2008), the antimicrobial property (Xing, Yang, & Dai, 2007), and photocatalytic activity (Daoud & Xin, 2004), respectively.

Xing and Ding (2007) applied the sol-gel surface modification to improve the UV photostabilization of Kevlar® fibres. TiO_2 nanosols were prepared by using tetrabutyl titanate as precursor. In their following work, Al^{3+} doped TiO_2 coating was applied on Kevlar® fibres to improve the photostabilization by sol-gel method (Li, Xing, & Ding, 2007). In the sol-gel preparation, Al^{3+} was added to lower the photocatalytic activities of TiO_2. This special treatment to the sol-gel preparation improved the photostabilization of Kevlar® fibres against UV radiation by retaining about 69% tensile strength after 60 hours exposure compared to 65% from their previous work.

THE PRACTICAL METHODS TO STUDY PHOTOSTABILITY

To study polymer photostability, various methods and approaches are applied in the degradation simulations and examination of properties from the macro perspective to the micro perspective. These methods commonly include: natural or artificial weathering, mechanical testing, and morphology study by using various microscopes, oxygen-uptake measurements, and molecular weight changes in the degradation process.

The natural and artificial weathering of polymers has been introduced in the previous section. Natural weathering is much closer to real situations than artificial weathering. However, natural weathering is time consuming, unpredictable due to weather conditions and difficult to replicate. Artificial weathering is more widely used because it can reduce the testing time and control the experiment parameters.

Tensile strength is a mechanical parameter that on a gross level will indicate the

degradation degree. As the bonds within the polymer chains break during degradation, the tensile strength normally decreases. Loss of tensile strength is widely used in studies of the degradation of fibres (Yang & Ding, 2006; Chung & Herold, 1991; Morton, 1974; Johnson, Tincher & Bach, 1969) and fabrics (Brown *et al.*, 1983). Elongation at break is another mechanical estimation for degradation. Torikai *et al* (1990) evaluated the factors affecting the photostability of polyethylene by testing the elongation at break of the polyethylene (PE) films after irradiation. The elongation at break decreased after irradiation.

A possible change of fabrics after light radiation is the color yellowing. Millington studied the affecting factors, experimental techniques, photochemical mechanism and prevention methods about photoyellowing of wool (2006a & 2006b). Aramid films were reported that a yellowing happened on the first few microns of the film surface facing the ultraviolet source under vacuum irradiation (Carlsson *et al.*, 1978a). The probable cause of color yellowing is the formation of blue compounds, such as polyenes from organic materials (Grattan, 1978). To compare the yellowing index of the samples before and after radiation is an approach to evaluate the degradation degree (Montazer & Pakdel, 2010).

Fourier transform infrared spectroscopy (FTIR) works on the fundamental principle that molecules absorb specific frequencies of electromagnetic waves that can be used to characterize the structure. An absorption spectrum is formed to identify the corresponding bond to the absorbance peak. Infrared spectroscopy is used to identify the yield during the degradation process (Wilkie, 1999; Villar-Rodil, Paredes, Martinez-Alonso, & Tascon, 2001).

X-ray photoelectron spectroscopy (XPS) applies a beam of X-rays incident on a

sample surface. The ejection of photoelectrons from the top 300 nm of the sample surface is measured. Though it requires an ultra high vacuum-working environment, XPS is one of the most useful techniques. Its high sensitivity makes it an effective probe for surface detection and also bulk material study. It is widely used to determine the elemental composition of the surface, chemical or electronic state of each element in the surface or bulk of pure materials. In the study of material degradation, XPS is often used to examine the yield of carboxylic acid (−COOH) groups on the surface of a material (Hamilton *et al.*, 1993; Xing & Ding, 2007) and the deposition of photostabilizer (Xing & Ding, 2007; Pandey *et al*, 2009).

X-ray diffraction analysis (XRD) works in a way that X-rays incident on a group of atoms will excite the electrons. The scattering wave emitted from atomic layers creates interference effects and leads to the diffraction phenomena. The density of the diffracted beam is determined by the relative arrangement of atoms within a unite cell and the scattering power of single atoms. XRD is often used to determine the crystallinity of polymers. The increase in crystallinity of radiated polypropylene samples was found by using XRD (A. Gupta, Saroop, & V. Gupta, 2007).

Energy-dispersive X-ray spectrometry (EDS) is a technique to analyze the elemental and chemical characterization of a sample. It relies on the fundamental principle that each element has a unique atomic structure to emit X-rays as a characteristic to identify it from other elements. It is usually used to identify the elements in and particle size of the coatings (Montazer & Pakdel, 2010).

Various types of microscopes are an important approach to investigate the surface

morphology changes after degradation. They are also effective to observe the structural characteristics of coatings. Scanning electron microscopy (SEM) applies an electron beam to form an image of the sample morphology. It is widely used to study the structural and surface characteristics due to its high resolution and depth of focus. The requirement of the sample in SEM is clean, dry, vacuum compatible and electrically conductive. It is a common and useful tool in analyzing coatings (Xing & Ding, 2007; Abidi *et al.*, 2007). Environmental scanning electron microscope (ESEM) can be seen as a updating of conventional SEM. It offers the functions of conventional SEM and also allows the direct observation of unprepared, wet or oil specimen, and even dynamic process (Wei, Wang, Mather & Fotheringham, 2004). The operating principle of transmission electron microscopy (TEM) is that a beam of electron transmits through a thin sample. The sample absorbs the electrons. The transmitted electrons will strike on a fluorescent screen and form an image that darker screen areas show regions of more absorption of the electron. TEM usually provides a high-resolution image. It is a useful tool to study the material morphology, especially for coatings to evaluate the particle dispersion (Sójka-Ledakowicz *et al*., 2008). Atomic Force Microscopy (AFM) is a kind of scanning probe microscope with a high resolution. The information on the surface morphology is gathered in this way. AFM uses a cantilever stylus with a tip radius on the order of nanometer. When such a tiny tip contacts with the surface, forces between the tip and the atoms of the sample causes deflection of the cantilever. This deflection is measured by using a laser beam reflected from the cantilever top. AFM provides a three-dimension image of the morphology and it does not require any kind of special treatment of the surface that may damage the original morphology. In their study of Nomex® aramid fibres, Villar-Rodil *et al* (2001) used AFM images to show the morphology difference among the samples caused by thermal degradation.

The direct impact of degradation to polymers is the decrease of molecular weight by the breaking of bonds and long chain molecular scission. Polymer molecular weight can be classified as number-average molecular weight, weight-average molecular weight, viscosity-average molecular weight and z-average molecular weight. The viscosity average molecular weight of Kevlar® yarns was measured and small decreases were observed after 60 days of sunlight radiation (Brown *et al.*, 1983). In the study of degradation kinetics of polyamides, authors observed the weight-average and number-average molecular weight, respectively. Both showed the molecular weight decreasing with time (Horta, Coca & Díez, 2003).

Oxygen uptake is a method that can track the oxygen consumption during the degradation process. Oxygen uptake is reported as an index to evaluate the degradation degree (Gijsman *et al.*, 1999). Oxygen is normally consumed during polymer degradation. Hydroperoxides are usually the yields of the oxidation of polymers. In Fraisse *et al*'s study, it was found that the oxygen consumption increased with the radiation exposure time and there was a linear correlation between the oxygen consumption and hydroperoxides content in pure oxygen (Fraïsse, Kumar, Commereuc & Verney, 2006).

The ultraviolet protection factor (UPF) is an index to evaluate the UV protective properties of textiles. It is defined as the ratio of the average effective UV irradiance calculated for unprotected skin to the average effective UV irradiance calculated for skin protected by the test fabric (Hoffmann *et al.*, 2001). Fabric porosity, weight, thickness, color and the presence of UV absorbers would affect the UPF of a fabric. Titanium dioxide as a UV blocking additive was coated on cotton fabrics, which enabled the UPF to improve a lot (Yang *et al*., 2004).

CHAPTER 3 METHODS

This chapter introduces the materials and equipment used, as well as the analytical methods applied on the sol-gel coated aramid fabrics. The sol-gel coating process includes sol solution preparation, padding and drying. Then the titanium dioxide (TiO_2) sol-gel coated fabrics are obtained. To evaluate the coating effects, the tensile properties of fabrics are determined, including breaking strength and elongation at break. Next, the chemical composition changes of fibres and the crystalline form of TiO_2 film are studied by X-ray photoelectron spectroscopy (XPS) and X-ray diffraction (XRD), respectively. At last, the surface morphology of coated fabrics is evaluated by scanning electron microscopy (SEM).

MATERIALS AND EQUIPMENTS

Aramid fabrics

Plain woven greige Nomex® fabrics with different mass were selected to receive the sol-gel coating. These greige Nomex® fabrics were provided by DIFCO Performance Fabrics Inc., Montreal, Canada. Table 2 shows the fabrics specifications.

Table 2. Fabric specifications

Fabrics	Mass[a] (g/m^2)	Thickness[b] (mm)	Fabric count[c] (W/cm×F/cm)
A	183.9	0.68	22×17
B	196.5	0.62	26×18
C	254.8	0.66	25×19

[a]CAN/CGSB 4.2 NO.5.1-M90(2004)
[b]CAN/CGSB 4.2 NO.37-2002(2002) (Small diameter foot, 1.0kPa)
[c]CAN/CGSB 4.2 NO. 6-M89/ISO 7211/2:1984 (1989) (Method C)

Greige Nomex® fabrics were delivered on manufacturer-provided fabrics rolls.

They were cut into 800 mm × 300 mm, swatches with lengthwise dimension in the warp direction to fit the coating equipment. Then these greige Nomex® fabrics were washed according to AATCC Test Method 135-2004 (2007). After been washed, they were ironed flat and smooth. Then these fabrics were stored in black plastic bags without light radiation in a conditioning room (20 ± 2°C, 65 ± 2% RH) until they received the sol-gel coating. These uncoated fabrics were defined as original fabrics in this study.

Sol-gel coating

Sol-gel coating on greige Nomex® fabrics was conducted at Tianjin Polytechnic University, China. The coating process included sol solution preparation, padding and drying. The process is simply illustrated in Figure 6. A lyogel is an aqua gel while a xerogel is a dried gel from lyogel (Brinker & Scherer, 1990).

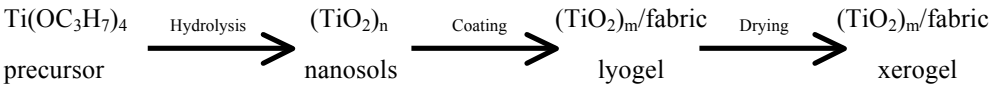

Figure 6. Main steps for TiO_2 sol-gel coating

The precursor of the titanium dioxide sol-gel used in this study was titanium isopropoxide $Ti(OC_3H_7)_4$ and the solvent was 95% ethanol. Titanium isopropoxide was purchased from Fisher Scientific, USA. Ethanol was purchased from Tianjin Fengchuan chemical reagents scientific company, China. Nitric acid HNO_3 from Tianjin Fengchuan chemical reagents scientific company was used to control the pH value of the solution. Two concentrations of sol solutions were used. Table 3 shows the descriptions of the sol solutions.

Table 3. The descriptions of sol solutions

Solution	A	B
Concentration (mol/L)	0.827	0.414
Molar ratio (precursor:solvent)	1:16	1:32
pH value	≈3	≈3

Firstly, ethanol was placed in a 2-litre beaker (Figure 7), and several drops of concentrated nitric acid were added into ethanol to adjust the pH value to about 3. Then titanium isopropoxide was added drop-wise over a period of 4 hours under strong and constant stirring. After stirring, a homogeneous sol-gel solution with a blue gloss was produced. The sol solution preparation is illustrated in Figure 7.

Figure 7. The preparation of sol-gel solution

Padding and drying

The fabric was immersed in the sol solution for 30 seconds, then passed through pad rollers with a pressure of 2.75kgf/cm^2. The wet fabric was dried in an oven at 60°C for 5 minutes and cured at 100°C for 3 minutes. Figure 8 and 9 show the padding and drying equipment. After the coating process, the fabrics were stored in black plastic bags to eliminate light radiation.

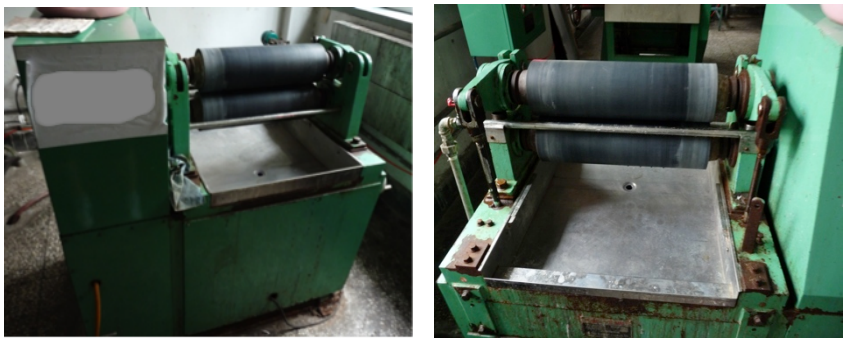

Figure 8. The padder roller at Tianjin Polytechnic University, China

Figure 9. The drying oven at Tianjin Polytechnic University, China

ANALYTICAL METHODS

Add-on Weight Measurement

The coatings increased the mass of fabrics. The add-on weight percent is calculated as:

$$\text{Add-on weight percent (\%)} = 100(M-m)/m \qquad \text{Eq (2)}$$

where M= mass of coated fabric sample,

m= mass of original uncoated fabric sample.

The mass of the coated fabrics was determined according to standard method CAN/CGSB4.2 NO.5.1-M90 (2004).

Accelerated Photodegradation Experiments

The original and coated samples were exposed to light radiation in an Atlas xenon arc Weather-Ometer according to AATCC Test Method 16-2004 Option 3 (2007). The Atlas xenon arc Weather-Ometer used a water-cooled xenon lamp with a borosilicate inter glass filter and soda-lime outer filter to give a spectral distribution similar to that of sunlight passed through a window glass (Figure 10). It simulated solar radiation and provided a full spectrum of light irradiance of 1.1 W/(m^2nm) at 420 nm (Figure 11). The black panel temperature was 63°C. The dry bulb temperature was 30°C and relative humidity was 30%. Since the exposure time of one hour was not exactly equal to one AATCC Fading Unit (AFU), some extra hours were run to meet the standard of one AATCC Fading Unit. Figure 10 shows images of the weather-ometer in the Department of Human Ecology, University of Alberta.

(a) Weather-Ometer (b) Sample holders

Figure 10. Atlas xenon arc Weather-Ometer at University of Alberta

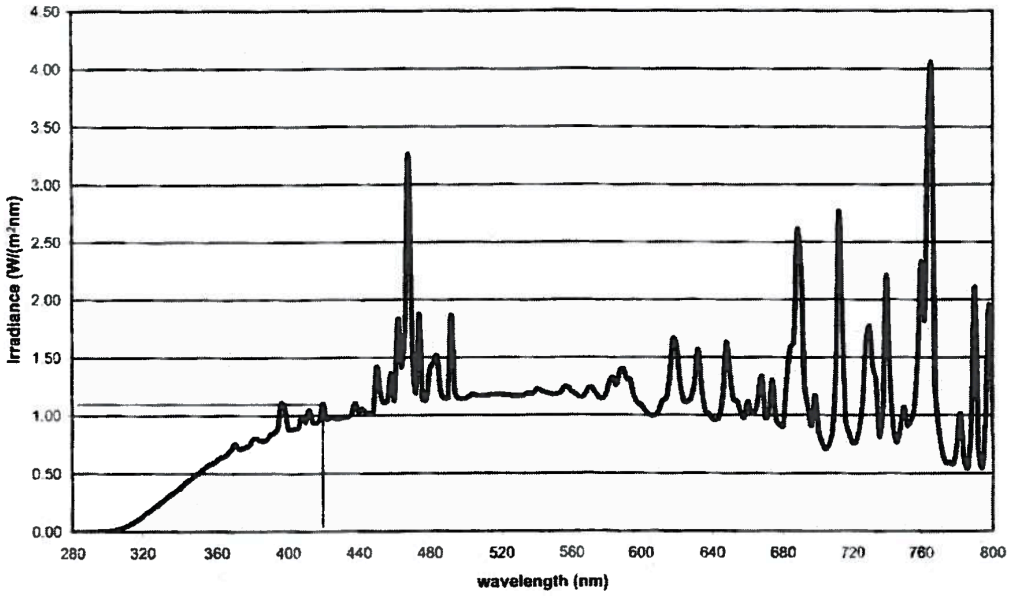

Figure 11. Filtered xenon lamp spectral power distribution controlled at 1.1W/(m^2nm) at 420 nm (AATCC 16-2004, 2007)

Five specimens each of coated sample and original control were cut to the size of 150 mm × 35 mm with the lengthwise dimension in the warp direction. Then the specimens were placed in an aluminum frame with one side of the fabric exposed to the xenon arc radiation (Figure 12). Due to experimental constraints and in order to use energy efficiently, a running time schedule was applied (Table 4).

Table 4. Exposure time schedule and irradiance record during exposure

Test Interval (AFU)	Irradiance (KJ/m^2/nm)	Average irradiance per AFU (KJ/m^2/nm)	Manipulations
40.0	170.9	4.27	Before beginning: put in 40, 80, 120 AFU specimens After end: get out 40 AFU specimens
40.0	169.8	4.25	Before beginning: put in 60 AFU specimens After end: get out 80 AFU specimens
20.0	85.0	4.25	Before beginning: put in 20 AFU specimens After end: get out 20 AFU and 60 AFU specimens
20.0	85.0	4.25	After end: get out 120 AFU specimens

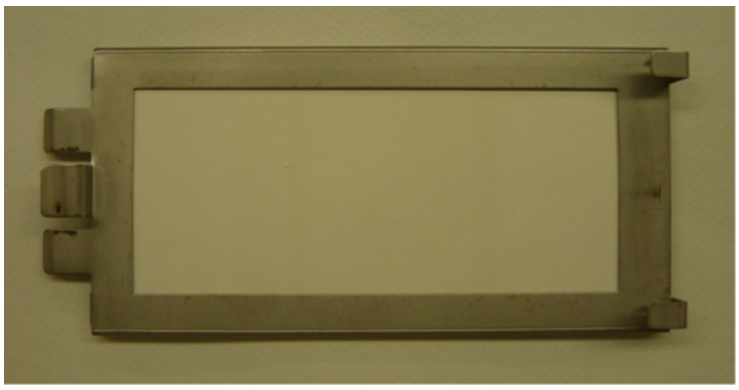

(a) Aluminum frame

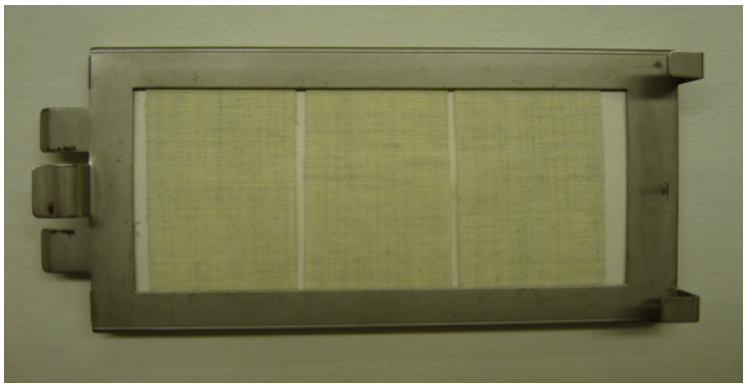

(b) Aluminum frame with fabric strips

Figure 12. Aluminum frame and fabric strips for photodegradation experiment

Instron breaking strength testing

The breaking strength of both coated and original uncoated specimens after exposure was measured by an Instron tensile testing instrument. Instron tensile testing was carried out in a conditioning room (20 ± 2°C, 65 ± 2% RH). Testing method CAN/CGSB 4.2 NO.9.1-M90 (2004) was followed, using the ravel strip method. Each specimen was cut into 150 mm × 35 mm strips with the longer dimension in the warp direction. Then the specimen was ravelled to a width of exactly 25 mm by removing approximately the same number of yarns from each side of the strip. Five replicates per treatment were tested on an Instron constant-rate-of-extension (CRE) tensile testing equipment (Figure 13).

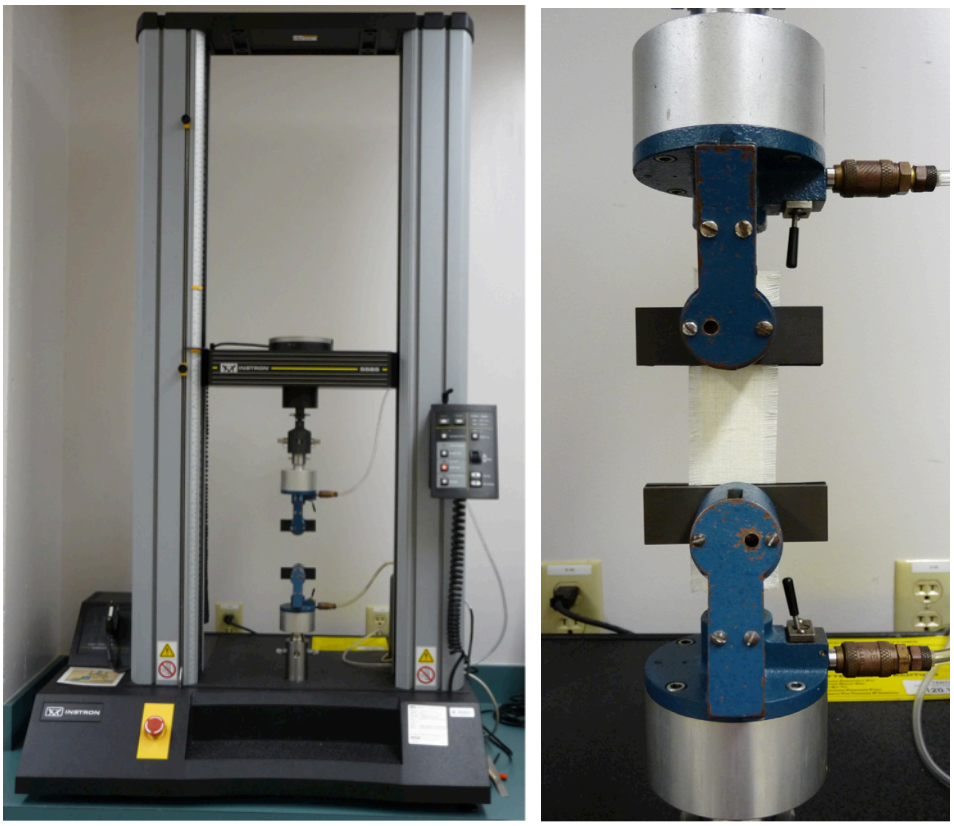

(a) (b)

Figure 13. Instron tensile testing instrument ((a) Instron tensile testing instrument, (b) clamps with a raveled fabric strip)

X-ray photoelectron spectroscopy (XPS)

The chemical composition of original and coated fabric before and after accelerated photodegradation was evaluated by X-ray photoelectron spectroscopy. Room-temperature XPS experiments were performed at the Alberta Center for Surface and Engineering Science (ACSES) using a Kratos Axis 165 spectrometer with monochromatized Al K_α ($h\upsilon$ = 1486.71 eV). The spectrometer was calibrated by the binding energy (84.0 eV) of Au $4f_{7/2}$ with reference to Fermi level. The pressure of the analysis chamber during experiments was better than 5×10^{-10} Torr. A hemispherical electron-energy analyzer working at the pass energy of 20 eV was used to collect core-level spectra while a survey spectrum within a range of

binding energies from 0 to 1100 eV was collected at an analyzer pass energy of 160 eV. Charge effects were corrected by using the C 1*s* peak at 284.8 eV.

A Shirley curve background was applied to subtract the inelastic background of core-level peaks. Non-linear optimization using the Marquardt Algorithm was used to determine the peak model parameters such as peak positions, widths and peak intensities. The model peak to describe XPS core-level lines for curve fitting was a product of Gaussian and Lorentzian functions (Casa XPS, 2006).

X-ray diffraction (XRD)

The crystalline form of titanium dioxide on the coated fabrics was examined by X-ray diffraction (XRD) using a Rigaku Ultima IV unit in the Department of Earth and Atmospheric Science, University of Alberta. The unit applied a D/Tex detector with Fe filter and Cobalt radiation tube at 40kV and 40mA (λ=1.79026Å). Samples were run using a top-pack mount at a speed of 2 degrees 2-theta per minute with a step size of 0.02 degrees. Samples ran from 5° to 90° on a continuous scan.

The crystalline size of TiO_2 is calculated according to Equation (3) (Montazer & Pakdel, 2010):

$$\text{Crystal size (Å)} = \frac{K \times \lambda \times 180}{FWHM \times \pi \times \cos\theta} \qquad \text{Eq (3)}$$

Where K=0.9 is the shape factor, λ is the wavelength of X-ray of Cobalt radiation, FWHM is full width at half maximum of the peak and θ is the diffraction angle.

Scanning Electron Microscopy (SEM)

Surface appearance of both original uncoated and coated fabric was investigated using scanning electron microscopy in the Department of Earth and Atmospheric Science, University of Alberta.

Fabric specimens were cut into small circles and mounted on stubs. The stub edge and fabric edge were coated with Pelco® colloidal silver liquid. The specimens were coated with gold by using a Nanotech SEMPrep 2 DC sputter coater. A JEOL 6301F field emission scanning electron microscope was used to capture the morphology images of fabric specimens, specially the surface appearance of original uncoated and coated fabric and fibre before and after accelerated photodegradation and tensile strength testing. The secondary electron images were obtained using a Everhart-Thornley detector. Working distance ranged from 15 mm to 17mm and the accelerating voltage was 5.0 kV to obtain images. The magnifications are listed at the bottom of each image.

CHAPTER 4 RESULTS AND DISCUSSION

Add-on weight

The add-on weight of TiO_2 on the coated Nomex® fabric is listed in Table 5. For a specific mass fabric, the high concentration sol solution coating resulted in a higher add-on weight than the low concentration sol solution coating did under the same roller padding pressure of 2.75kgf/cm^2. For both the low and high concentration coatings, the low mass fabric gained a higher add-on weight than the heavier fabric did under the same roller padding pressure.

Table 5. Add-on weight of TiO_2 on the coated Nomex® fabric

	Original mass[a]	Low concentration coating		High concentration coating	
	(g/m^2)	Mass[a](g/m^2)	Increase (%)	Mass[a](g/m^2)	Increase (%)
A	183.9	196.2	6.7	200.8	9.2
B	196.5	207.9	5.8	212.2	8.0
C	254.8	264.0	3.6	272.4	6.9

[a]CAN/CGSB 4.2 NO.5.1-M90(2004)

Once the fabric was immersed in sol solution, fibres on the fabric surface got wet at once and the fibres underneath started to get wet by capillary forces (Krüger, Bockmeyer, Dutschke, & Löbmann, 2006). The gaps between the fibres were also completely filled with sol solution liquid. Wet fabrics were put through a pad roller to force the liquid to drain and remove the extra. For a high concentration sol solution, the number of nanometre-sized particles per unit volume is larger than low concentration sol solution. After drying, the particles condensed and formed into films on the surface of fibres and also in the gaps between individual fibres. As result, the high concentration sol solution developed a higher add-on weight than the low concentration sol solution. A loosely woven fabric tends to

hold more of the sols between its fibre gaps than tightly woven fabric. After the drying process, the film that formed between the gaps contributed a large proportion of the add-on weight.

In the study by Krüger *et al* (2006), a "three-fibre" model for film formation and fibre bridging in sol-gel coating on fabric was presented. During the drying and curing process, the solvent evaporated and the sol solution underwent shrinkage on the fibre surface. The gaps filled with sol solution in the dipping became empty. During the emptying of the gaps, menisci were formed (Krüger *et al*., 2006). The bridging between the fibres would affect the stiffness and mechanical properties of the coated fabric.

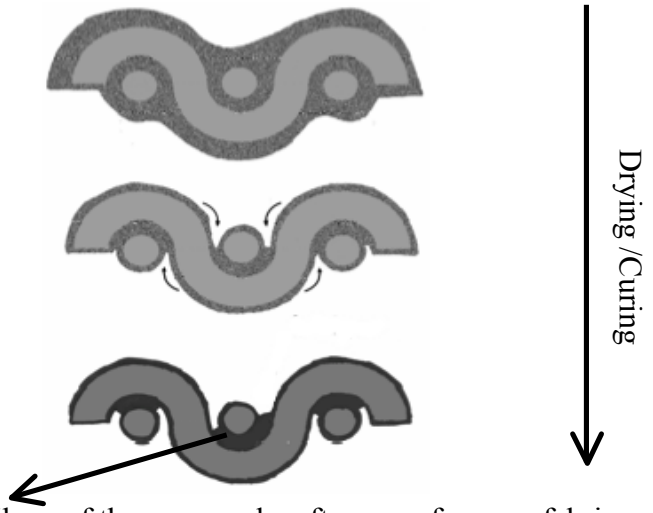

Figure 14. Krüger *et al*'s model for film formation and fiber bridging during drying process (as cited in Mahltig & Textor, 2008)

Breaking strength and photodegradation rate

Table 6 presents the mean breaking strength (n=5) of the original uncoated fabrics with respect to light exposure in the weather-ometer.

Table 6. Breaking strength (n=5) of original uncoated fabrics vs. light exposure

Light exposure (AFU)	A (184g/m^2) Maximum Load (N)	B (196g/m^2) Maximum Load (N)	C (255g/m^2) Maximum Load (N)
0	438.3	584.3	565.7
20	367.1	489.1	480.1
40	298.4	389.2	390.0
60	251.5	342.8	340.1
80	221.6	298.3	297.8
120	180.6	249.2	240.8

Table 7. Retained breaking strength (%) of original uncoated fabrics vs. light exposure

Light exposure (AFU)	A (184g/m^2) Maximum Load (%)	B (196g/m^2) Maximum Load (%)	C (255g/m^2) Maximum Load (%)
0	100	100	100
20	83.7	83.7	84.9
40	68.1	66.6	68.9
60	57.4	58.7	60.1
80	50.6	51.0	52.6
120	41.2	42.6	42.6

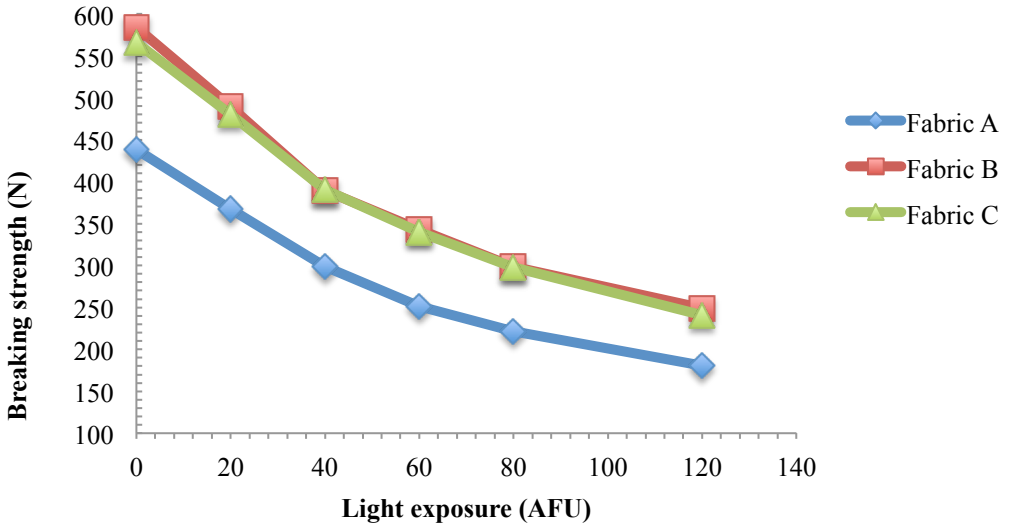

Figure 15. Breaking strength (n=5) of original uncoated fabrics vs. light exposure

The initial breaking strengths before radiation of fabric B and fabric C are very close (584.3N and 565.7N, respectively) because of their close fabric count. During the entire light exposure, the breaking strength retained by the three fabrics was very similar (Table 7). After 120 AFU of exposure, the fabrics retained about 40% of their initial breaking strength.

Figure 15 shows the change of breaking strength with respect to the light exposure (AFU). The curves show that the change of breaking strength of the three original uncoated fabrics followed a similar pattern. It is assumed that the degradation of the Nomex® fabrics adheres to the same mechanism as that of nylon. The absorbed energy from light radiation broke the bonds along the fibre backbone. For Nomex® fibres, these broken bonds are mainly the −CO−NH− bonds, which caused the loss of breaking strength (Carlsson *et al*., 1978b).

The slope of the breaking strength curve shows the photodegradation rate (Newton/AFU) of the fabrics during the accelerated photodegradation period. The photodegradation rate of the three fabrics at different exposure intervals is shown in Figure 16 to 18. The entire radiation exposure period is divided into three intervals: 0-40 AFU, 40-80 AFU, and 80-120 AFU. The photodegradation rate at each exposure interval is calculated from the corresponding change in breaking strength.

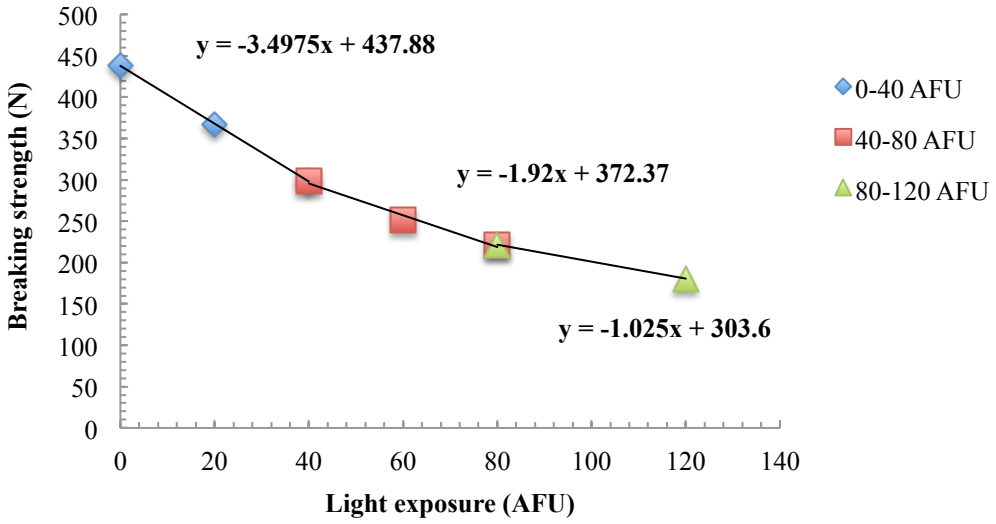

Figure 16. Determination of the photodegradation rate (N/AFU) of fabric A at different exposure intervals (0-40 AFU: 3.5N/AFU; 40-80 AFU: 1.9N/AFU; 80-120 AFU: 1.0N/AFU)

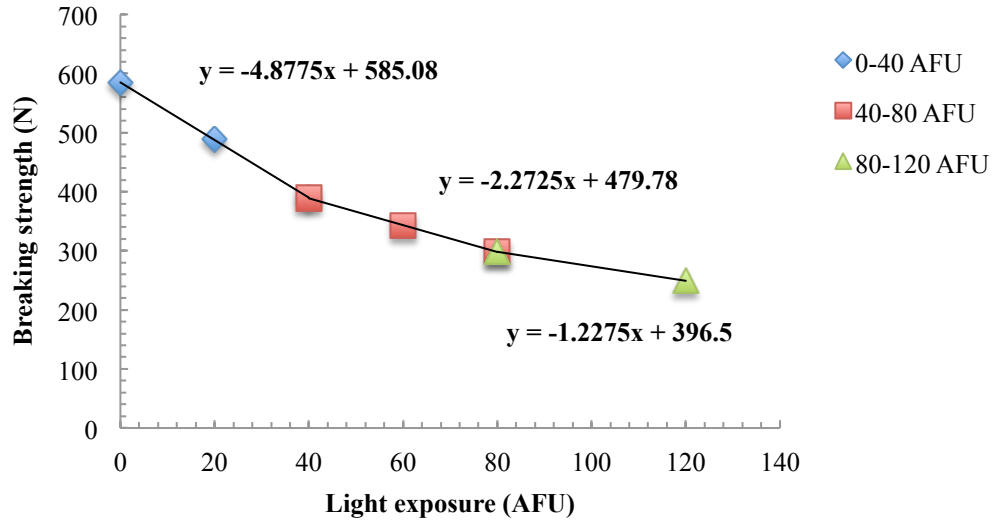

Figure 17. Determination of the photodegradation rate (N/AFU) of fabric B at different exposure intervals (0-40 AFU: 4.9N/AFU; 40-80 AFU: 2.3N/AFU; 80-120 AFU: 1.2N/AFU)

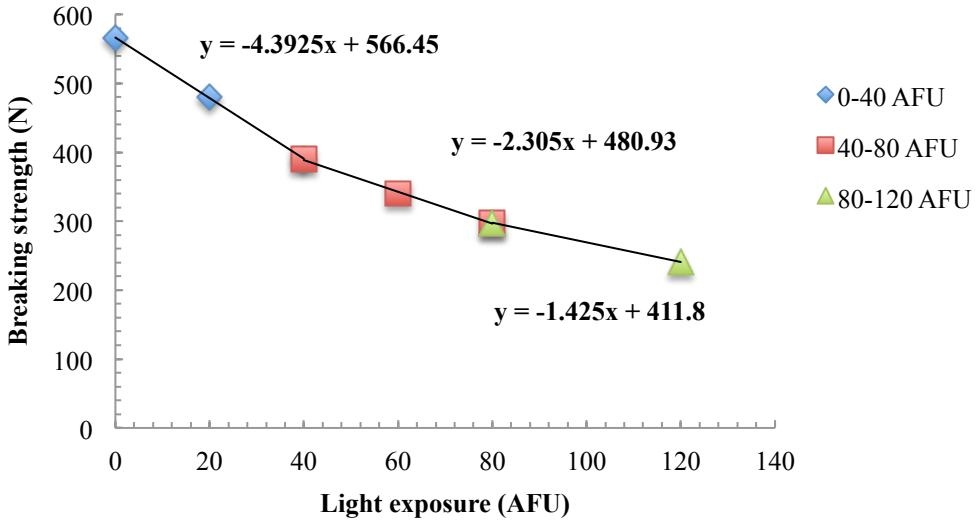

Figure 18. Determination of the photodegradation rate (N/AFU) of fabric C at different exposure intervals (0-40 AFU: 4.4N/AFU; 40-80 AFU: 2.3N/AFU; 80-120 AFU: 1.4N/AFU)

Table 8 and Figure 19 summarize the photodegradation rate of original fabrics at three exposure intervals. At 0-40 AFU, the degradation rate of the fabrics is about 4 N/AFU. The rate decreases to about 2 N/AFU at 40-80 AFU and to about 1 N/AFU at 80-120 AFU. This means that the photodegradation rate slows with the exposure time. This change can be interpreted as the Nomex® fibre forming a brown thin film on the surface to prevent the further degrading reaction (Dupont, 2001). The brown thin film is the photodegradation product of the polymer surface.

Table 8. Photodegradation rate (N/AFU) of original uncoated fabric at different exposure intervals

	Exposure Intervals (AFU)		
Fabric	0-40	40-80	80-120
A (184g/m^2)	3.5	1.9	1.0
B (196g/m^2)	4.9	2.3	1.2
C (255g/m^2)	4.4	2.3	1.4

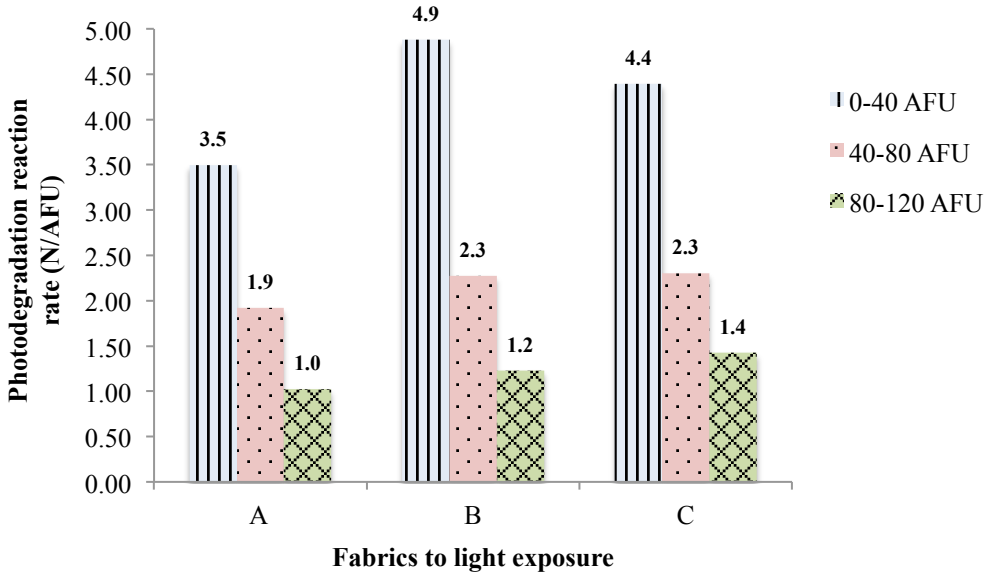

Figure 19. Photodegradation rate (N/AFU) of three original uncoated fabrics A (184g/m^2), B (196g/m^2) and C (255g/m^2) at three exposure intervals

The breaking strength of sol-gel coated fabrics are listed in following tables. The fabrics lost their breaking strengths to half of the original breaking strength after sol-gel coating both in high and low concentration sol solutions. Fabric A, for example, had an initial breaking strength of 438.3N (Table 9). However, the breaking strength decreased to 262.2N when coated with the low concentration sol-gel and 276.8N after coating with the high concentration sol-gel, respectively. The decrease also happened to fabric B and C (Table 10 & Table 11). This loss of breaking strength can be explained from two aspects.

Table 9. Breaking strength (n=5) of original uncoated, low concentration and high concentration sol-gel coated fabric A vs. light exposure

Light exposure (AFU)	Original uncoated Maximum Load (N)	Low concentration Maximum Load (N)	High concentration Maximum Load (N)
0	438.3	262.2	276.8
20	367.1	240.2	243.8
40	298.4	199.9	223.7
60	251.5	191.1	209.9
80	221.6	162.0	186.1
120	180.6	141.6	159.1

Original uncoated fabric A mass = 184g/m^2

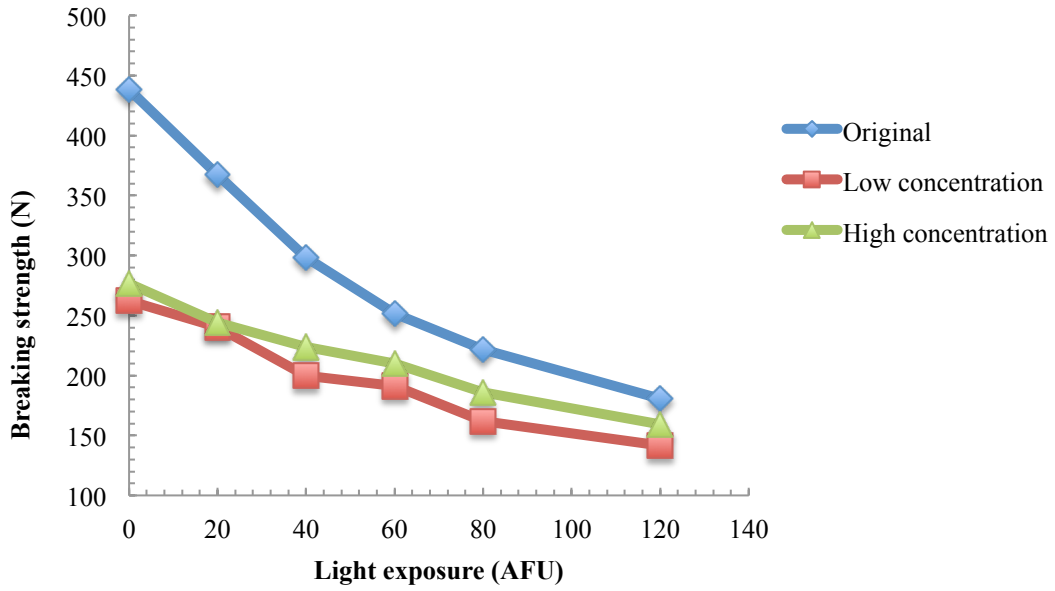

Figure 20. Breaking strength of original uncoated, low concentration and high concentration sol-gel coated fabric A vs. light exposure

Table 10. Breaking strength (n=5) of original uncoated, low concentration and high concentration sol-gel coated fabric B vs. light exposure

Light exposure (AFU)	Original uncoated Maximum Load (N)	Low concentration Maximum Load (N)	High concentration Maximum Load (N)
0	584.3	376.8	329.7
20	489.1	343.2	289.0
40	389.2	304.0	287.8
60	342.8	273.9	272.4
80	298.3	250.6	237.6
120	249.2	216.9	202.1

Original uncoated fabric B mass = 196g/m^2

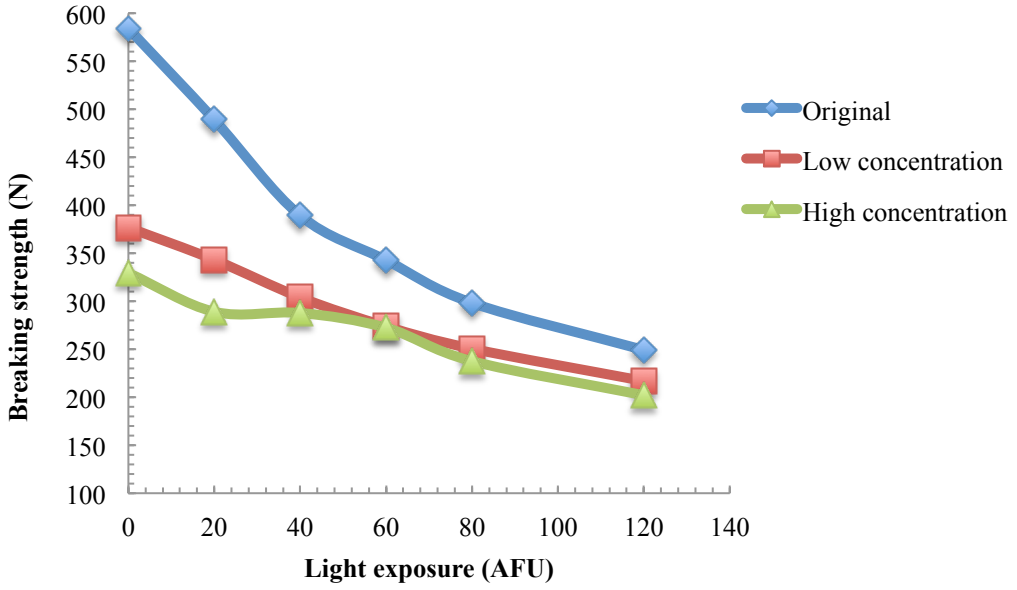

Figure 21. Breaking strength (n=5) of original uncoated, low concentration and high concentration sol-gel coated fabric B vs. light exposure

Table 11. Breaking strength (n=5) of original uncoated, low concentration and high concentration sol-gel coated fabric C vs. light exposure

Light exposure (AFU)	Original uncoated Maximum Load (N)	Low concentration Maximum Load (N)	High concentration Maximum Load (N)
0	565.7	315.5	337.3
20	480.1	267.3	308.7
40	390.0	241.3	274.9
60	340.1	229.0	259.1
80	297.8	202.1	234.3
120	240.8	176.9	205.3

Original uncoated fabric C mass = 255g/m^2

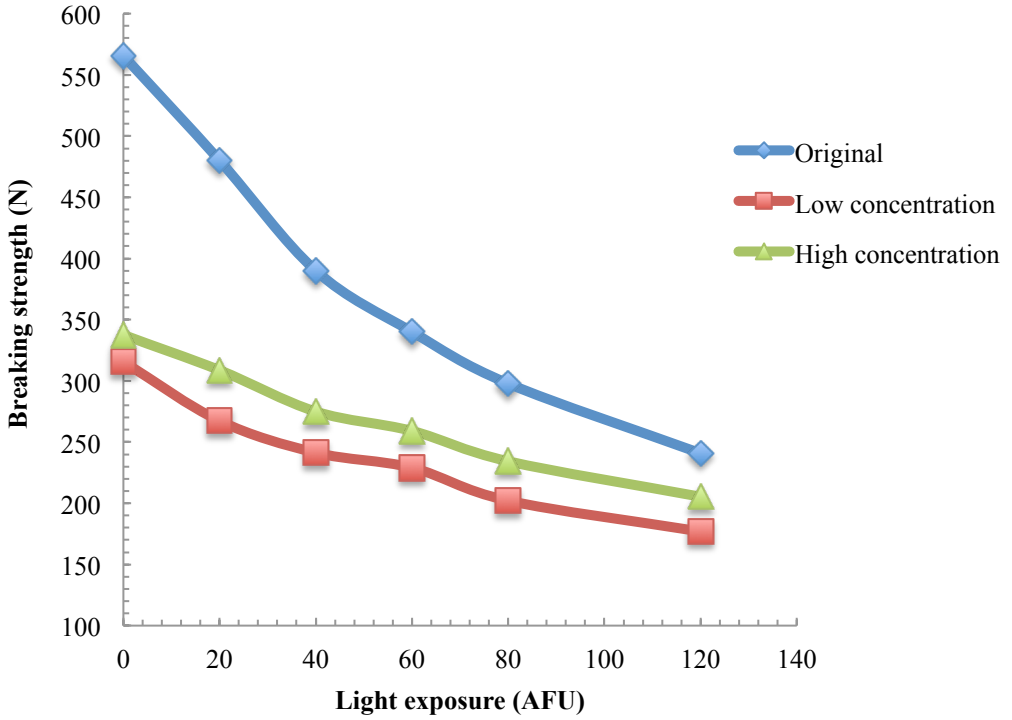

Figure 22. Breaking strength (n=5) of original uncoated, low concentration and high concentration sol-gel coated fabric C vs. light exposure

Firstly, the loss of breaking strength is caused by the structural change of the fabric. The film not only covers the fibre surface but also bridges the gaps between individual fibres (Figure 39). The fibres are stuck together by the inorganic TiO_2 thin film after sol-gel coating. The TiO_2 thin film decreases the flexibility of individual fibres. At the same time, the TiO_2 films increase the friction between single fibres (Mahltig & Textor, 2008). The inflexibility and the change in the fibre friction restrict the movement of the individual fibres. This reduction of the free movement prevents the readjustment of fibres when stressed, and therefore decreases the chance for fibres to join together to share the load when a load is applied. As result, fibres of the coated fabric tend to break at a lower load in comparison to original uncoated fabric while a load is applied.

A second contributing factor to the loss of initial breaking strength is the combined effect of the presence of nitric acid HNO_3 in the TiO_2 sol solution and the heat treatment afterwards. The purpose of using HNO_3 in the sol solution was to adjust the pH value at about three. This acidity is supposed to control the size of the TiO_2 particles on a nano scale (Su *et al*., 2004). Moreover, Nomex® fibre is reported to have a good resistance to acid higher than pH of two (Dupont, 2002), thus the TiO_2 sol-gel with pH value at three should not impair the Nomex® fabric. However, the heat treatment after the sol solution immersion (5 minutes at 60°C and 3 minutes at 100°C) enhanced the acidity of the gel by evaporating the solvent. The acidity of the gel on the fabric increased dramatically during the heat treatment. Under the high acidic environment, the acid would cause hydrolysis of amide linkages and loss of strength. It was reported that Nomex® fibre retained 60%-80% strength after exposure to 10% HNO_3 at 21°C for 100 hours (Dupont, 2001; Gabara *et al.*, 2006), however, 21°C is a much lower temperature than that used to cure the TiO_2 film.

The retained breaking strength (%) is the ratio of breaking strength of fabric with exposure to light to breaking strength of fabric without exposure. The retained breaking strength of original fabrics and coated fabrics without exposure are set at 100%. The retained breaking strength of fabrics with different exposure times are given in Table 12 to 14.

Table 12. Retained breaking strength (%) of original uncoated, low concentration and high concentration sol-gel coated fabric A vs. light exposure

Light exposure (AFU)	Original uncoated Maximum Load (%)	Low concentration Maximum Load (%)	High concentration Maximum Load (%)
0	100	100	100
20	83.7	91.6	88.1
40	68.1	76.2	80.8
60	57.4	72.3	75.8
80	50.6	61.8	67.2
120	41.2	54.0	57.5

Original uncoated fabric A mass = 184g/m^2

Table 13. Retained breaking strength (%) of original uncoated, low concentration and high concentration sol-gel coated fabric B vs. light exposure

Light exposure (AFU)	Original uncoated Maximum Load (%)	Low concentration Maximum Load (%)	High concentration Maximum Load (%)
0	100	100	100
20	83.7	91.1	87.6
40	66.6	80.7	87.3
60	58.7	72.7	82.6
80	51.0	66.5	72.1
120	42.6	57.6	61.3

Original uncoated fabric B mass = 196g/m^2

Table 14. Retained breaking strength (%) of original uncoated, low concentration and high concentration sol-gel coated fabric C vs. light exposure

Light exposure (AFU)	Original uncoated Maximum Load (%)	Low concentration Maximum Load (%)	High concentration Maximum Load (%)
0	100	100	100
20	84.9	84.7	91.5
40	68.9	76.5	81.5
60	60.1	72.6	76.8
80	52.6	64.1	69.5
120	42.6	56.1	60.9

Original uncoated fabric C mass = 255g/m^2

Figure 23 and 24 present the retained breaking strength of fabrics after light exposure to 60 AFU and 120 AFU. The retained breaking strength of original fabrics is about 42% after exposure to 120 AFU. After coating, the retained strength of fabric after exposure to 120 AFU increased to about 56% for low concentration sol-gel coating and 60% for high concentration sol-gel coating. This result indicates that the TiO_2 coating protected the fibres from the light radiation during the accelerated photodegradation. The high concentration sol-gel coating that generated a thick TiO_2 film on fibre surface provided a better protection than low concentration sol-gel coating.

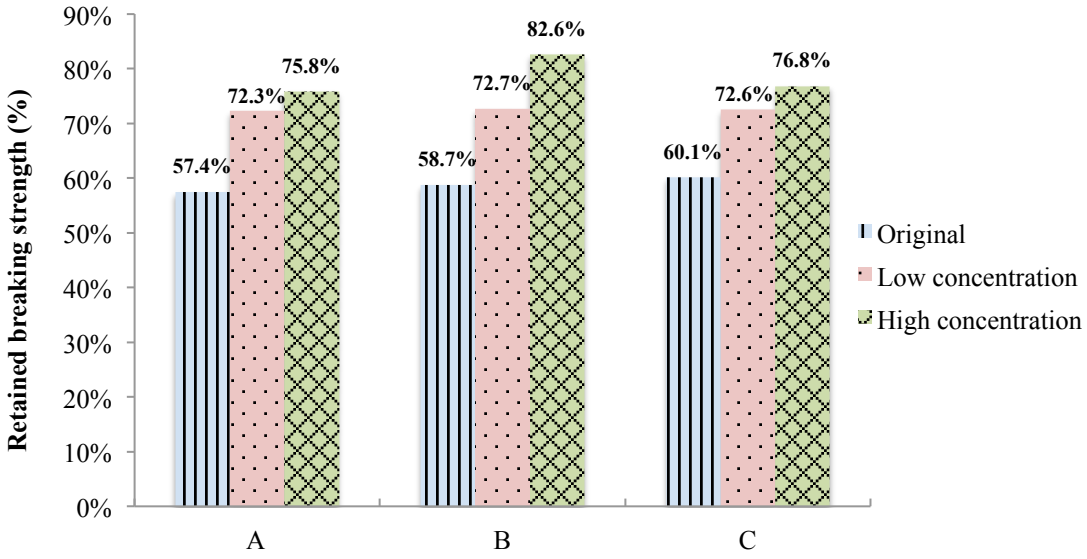

Figure 23. Retained breaking strength of fabric A (184g/m^2), B (196g/m^2) and C (255g/m^2) after exposure to 60 AFU

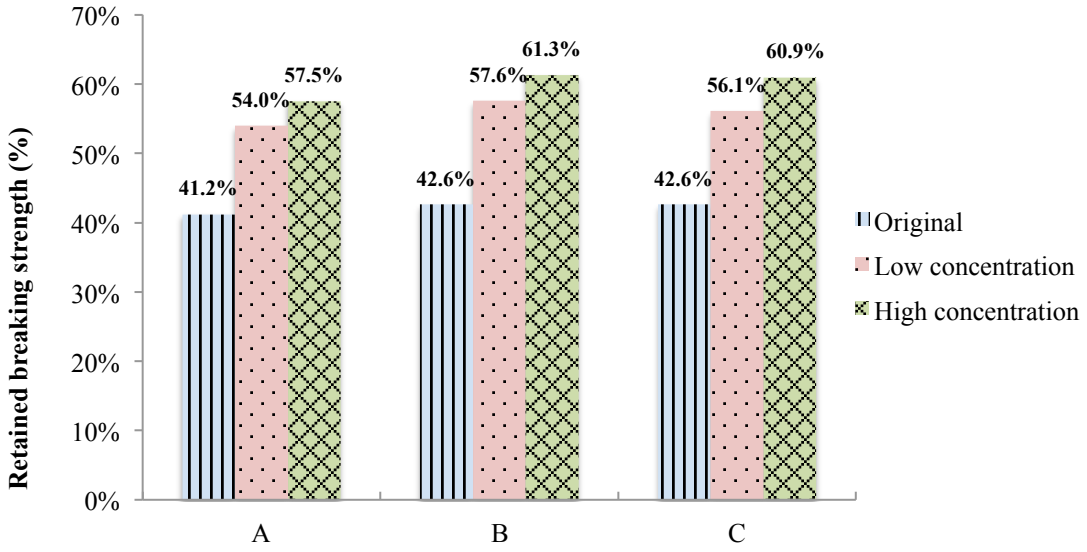

Figure 24. Retained breaking strength of fabric A (184g/m^2), B (196g/m^2) and C (255g/m^2) after exposure to 120 AFU

The primary cause for the improvement in retained breaking strength is that the TiO_2 film reduced the photodegradation rate. In order to evaluate the effectiveness of the TiO_2 film in slowing the photodegradation rate, the average reaction rate over the 120AFU exposure is displayed in Figure 25, 26,and 27.

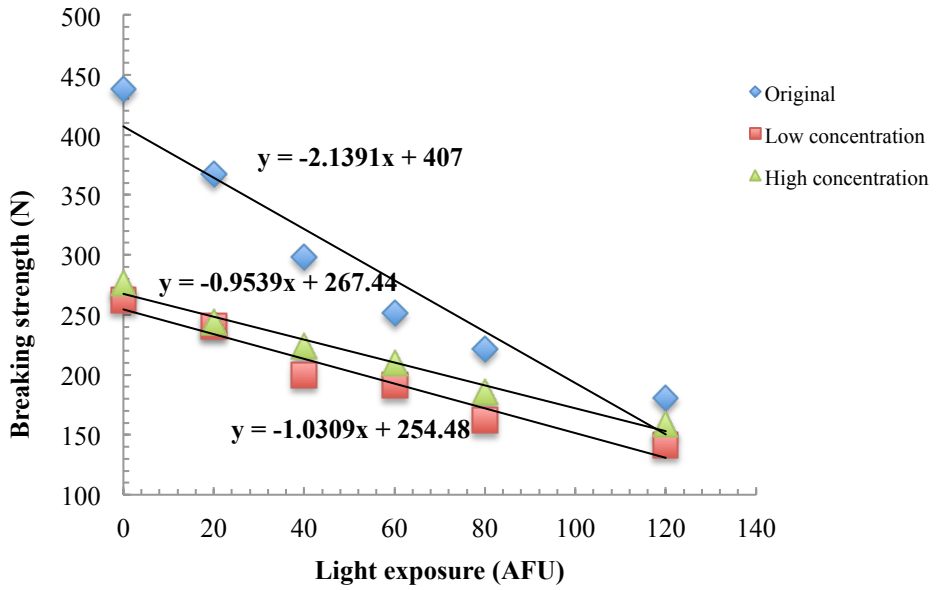

Figure 25. Linear relationship between breaking strength and light exposure for original uncoated and coated fabric A (184g/m^2)

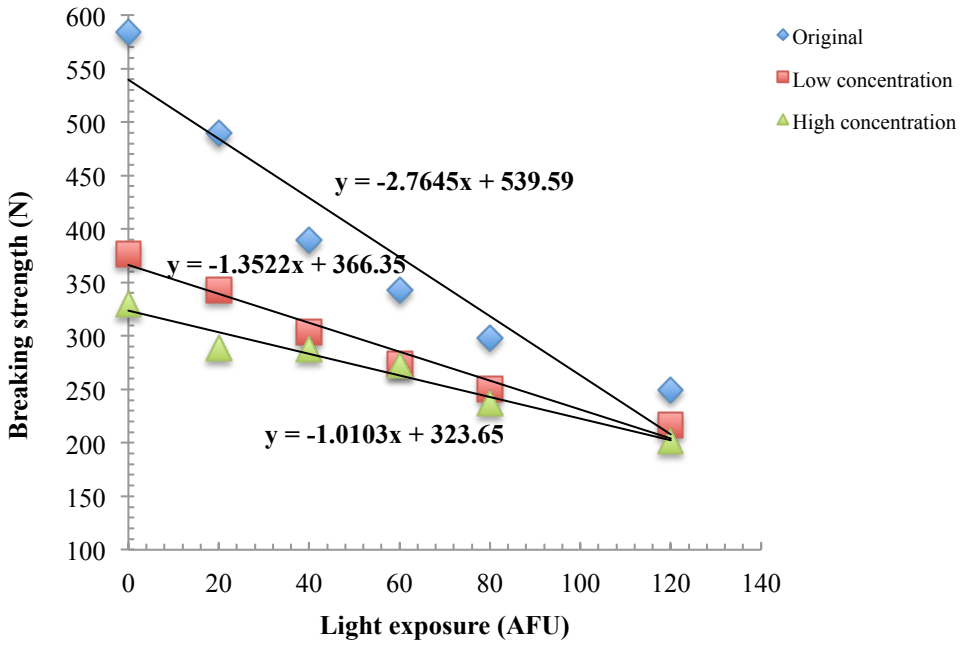

Figure 26. Linear relationship between breaking strength and light exposure for original uncoated and coated fabric B (196g/m^2)

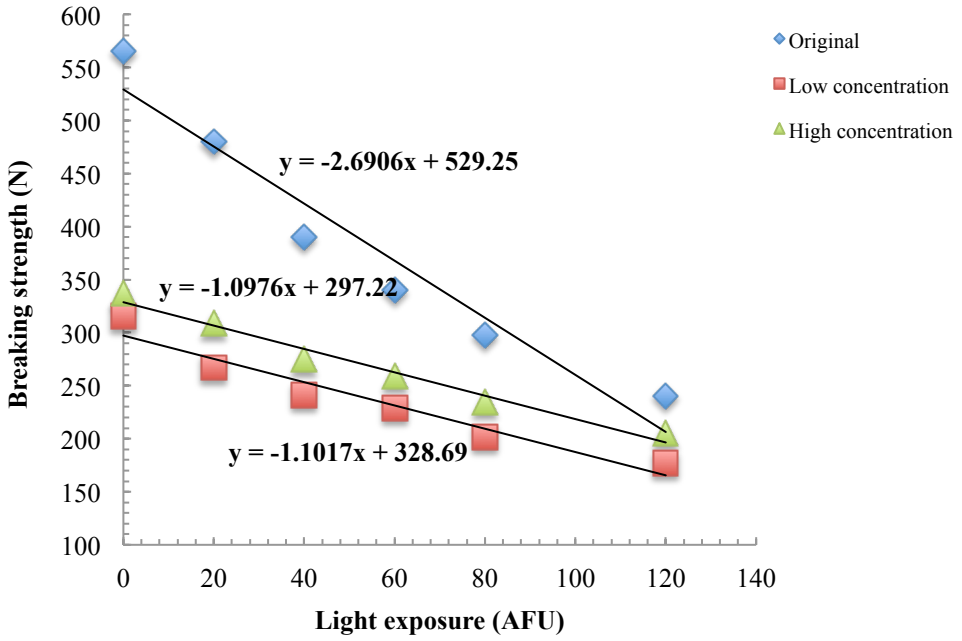

Figure 27. Linear relationship between breaking strength and light exposure for original uncoated and coated fabric C (255g/m^2)

Table 15. Photodegradation rate (N/AFU) of original uncoated and coated fabrics

	A	B	C
Original uncoated	2.1	2.8	2.7
Low concentration coating	1.0	1.4	1.1
Change percentage	-51.8%	-51.1%	-59.1%
High concentration coating	1.0	1.0	1.1
Change percentage	-55.4%	-63.4%	-59.2%

Change percentage (%) = 100 (original uncoated slope – coated slope)/original uncoated slope

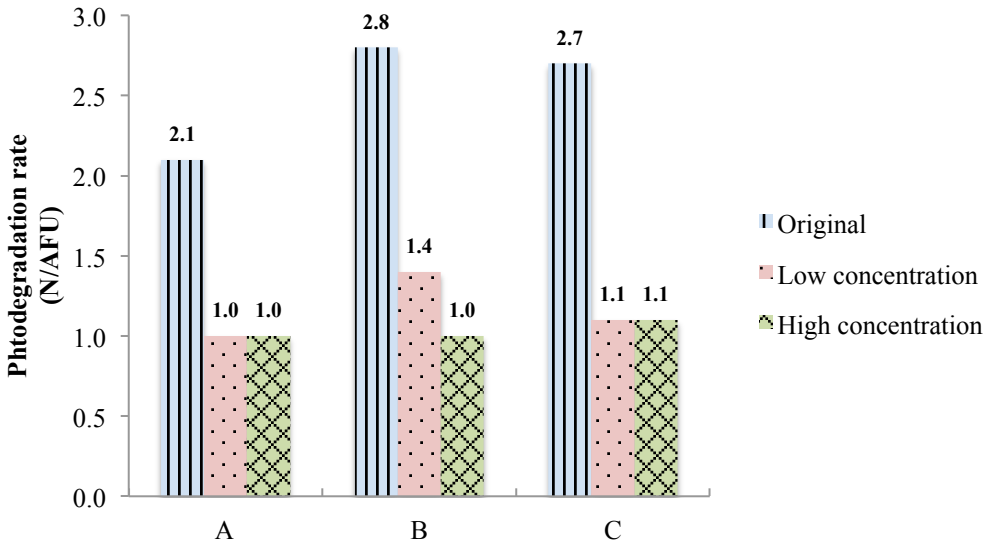

Figure 28. Photodegradation rate of original uncoated and coated fabric A (184g/m^2), B (196g/m^2) and C (255g/m^2)

Table 15 and Figure 28 are the average photodegradation rate of original uncoated and coated fabrics over the 120 AFU exposure. The results demonstrate that the applied TiO_2 film slowed the photodegradation rate. The reduced degradation rate of all three fabrics is over 50% and about 60% for the high concentration coating. However, in Figure 28 the data cannot demonstrate that there is any obvious difference between the protection action of low concentration coating and high concentration coating. A possible mechanism for how TiO_2 film slows the reaction rate can be interpreted by the Beer-Lambert law. The Beer-Lambert law explains the relationship between the property of the light absorption medium and the light intensity when light travels through the medium (Eq (4)) (Feller, 1994, p.56):

$$I=I_0 e^{-\alpha x} \qquad \text{Eq(4)}$$

where I_0 = Initial incident intensity, I = Intensity at depth x,

α = Absorption coefficient of the medium.

The TiO_2 film absorbed a certain amount of ultraviolet and visible light travelling through it. Hence, the TiO_2 film blocks the light arriving at the Nomex® fibre underneath the surface. As the quantum of photons arriving at the fibre surface decreased, the first step of photodegradation − that is the initiation, was slowed. Thus, the whole photodegradation rate was reduced.

Statistical analysis of breaking strength and photodegradation rate

The statistical analysis of breaking strength and photodegradation rate are given in Table 16 to 18. Table 16 shows the analysis of variance for each variable and their combinations influencing the breaking strength of fabrics. Differences were significant for all variables. The sol solution concentration had the most pronounced effect ($F_{2,216} = 6285.858$, $p \leq 0.001$) among all the variables.

Table 16. ANOVA test for significance of variables influencing breaking strength of fabrics

	df	SS	MS	F	$p \leq$
Weight	2	0.851	0.425	4079.310	0.000
Concentration	2	1.311	0.656	6285.858	0.000
Light exposure	5	2.387	0.477	4576.516	0.000
Weight/Concentration	4	0.087	0.022	208.717	0.000
Weight/Light exposure	10	0.005	0.001	5.198	0.000
Concentration/Light exposure	10	0.157	0.016	150.224	0.000
Weight/Concentration/Light exposure	20	0.009	0.000	4.201	0.000
Error	216	0.023	0.000		

ANOVA based on Log_{10} transformed data of breaking strength

The Tukey's groupings of significant differences of sol solution concentration and light exposure influencing the breaking strength of farbics are shown in Table 17. There is no significant difference between the breaking strength of the high concentration sol solution and low concentration sol solution coated fabrics without exposure ($x_H = 318.18$ N, $x_L = 314.60$ N) and exposure to 20 AFU ($x_H =$

283.56 N, x_L = 280.50 N). The breaking strength of high concentration sol solution coated fabric with exposure to 60 AFU (x_H = 247.13 N) has no significant difference from that of low concentration sol solution coated fabric with exposure to 40 AFU (x_L = 248.38 N). This means that the high concentration sol solution coated fabric is more photo stable than the low concentration sol solution coated fabric.

Table 17. Tukey's test for significance of sol solution concentration and exposure time influencing breaking strength of fabrics

Concentration × Light exposure	$\bar{x}$	n	Tukey's groupings*
Low × 120AFU	178.47	15	]
High × 120AFU	188.83	15	]
Low × 80AFU	204.90	15	]
High × 80AFU	219.36	15	]
Low × 60AFU	231.32	15	]
High × 60AFU	247.13	15	]
Low × 40AFU	248.38	15	]
High × 40AFU	262.14	15	]
Low × 20AFU	280.50	15	]
High × 20AFU	283.56	15	]
Low × 0AFU	314.60	15	]
High × 0AFU	318.18	15	]

* "]" means no significant difference in this grouping

With the increasing of the exposure time, there is a significant difference between the breaking strength of the high concentration sol solution and low concentration sol solution coated fabrics with exposure to 80 AFU (x_H = 219.36 N, x_L = 204.90

N) and 120 AFU (x_H = 188.83 N, x_L = 178.47 N). The effect of the sol solution concentration becomes more pronounced with the increasing of light exposure. Table 18 shows the analysis of variance for significance of sol solution concentration on photodegradation rate. Sol solution concentration was significant for photodegradation rate ($F_{2,6}$ = 41.640, $p \leq 0.001$). The sol-gel coating significantly improved the photostability of the aramid fabric.

Table 18. ANOVA test for significance of sol solution concentration influencing photodegradation rate

	df	SS	MS	F	$p \leq$
Concentration	2	4.179	2.089	41.640	0.000
Error	6	0.301	0.050		

Tensile extension and elongation at break

The elongation at break of fabric is another mechanical index to evaluate the photodegradation. The elongation at break is calculated according to Eq(5):

$$\text{Elongation at break (\%)} = (\Delta L/L_0)\times 100 \qquad \text{Eq(5)}$$

where ΔL = Tensile extension at break (mm),

L_0 = Initial length of fabric specimen (mm), here L_0 = 75 mm.

Table 19. Tensile extension (mm) at break of original uncoated, low concentration and high concentration sol-gel coated fabric A vs. light exposure

Light exposure (AFU)	Original uncoated ΔL (mm)	Low concentration ΔL (mm)	High concentration ΔL (mm)
0	42.85	25.83	25.74
20	32.26	23.95	22.83
40	25.05	18.29	20.35
60	21.09	17.37	19.26
80	19.54	14.84	17.00
120	16.33	13.48	15.02

Original uncoated fabric A mass = 184g/m^2

Table 20. Tensile extension (mm) at break of original uncoated, low concentration and high concentration sol-gel coated fabric B vs. light exposure

Light exposure (AFU)	Original uncoated ΔL (mm)	Low concentration ΔL (mm)	High concentration ΔL (mm)
0	45.54	27.30	24.41
20	33.90	25.62	21.33
40	26.89	21.73	21.94
60	23.15	19.16	20.68
80	20.63	17.64	17.87
120	18.48	15.34	15.83

Original uncoated fabric B mass = 196g/m^2

Table 21. Tensile extension (mm) at break of original uncoated, low concentration and high concentration sol-gel coated fabric C vs. light exposure

Light exposure (AFU)	Original uncoated ΔL (mm)	Low concentration ΔL (mm)	High concentration ΔL (mm)
0	55.63	30.05	32.69
20	44.93	26.56	29.78
40	36.95	22.93	26.50
60	32.62	22.06	24.12
80	29.07	18.89	22.16
120	26.19	16.78	18.83

Original uncoated fabric C mass = 255g/m^2

Table 22. Elongation at break (%) of original uncoated, low concentration and high concentration sol-gel coated fabric A vs. light exposure

Light exposure (AFU)	Original uncoated Elongation (%)	Low concentration Elongation (%)	High concentration Elongation (%)
0	57.1	34.4	34.3
20	43.0	31.9	30.4
40	33.4	24.4	27.1
60	28.1	23.2	25.7
80	26.1	19.8	22.7
120	21.8	18.0	20.0

Original uncoated fabric A mass = 184g/m^2

Table 23. Elongation at break (%) of original uncoated, low concentration and high concentration sol-gel coated fabric B vs. light exposure

Light exposure (AFU)	Original uncoated Elongation (%)	Low concentration Elongation (%)	High concentration Elongation (%)
0	60.7	36.4	32.5
20	45.2	34.2	28.4
40	35.9	29.0	29.3
60	30.9	25.5	27.6
80	27.5	23.5	23.8
120	24.6	20.5	21.1

Original uncoated fabric B mass = 196g/m^2

Table 24. Elongation at break (%) of original uncoated, low concentration and high concentration sol-gel coated fabric C vs. light exposure

Light exposure (AFU)	Original uncoated Elongation (%)	Low concentration Elongation (%)	High concentration Elongation (%)
0	74.2	40.1	43.6
20	59.9	35.4	39.7
40	49.3	30.6	35.3
60	43.5	29.4	32.2
80	38.8	25.2	29.5
120	34.9	22.4	25.1

Original uncoated fabric C mass = 255g/m^2

The changes of elongation at break of fabrics were similar to the changes seen in the breaking strength testing. The elongation at break of coated fabrics decreased in comparison to the original uncoated fabric. This can also be interpreted by the structural change of the fabric and the use of acid in the coating process. The elongation at break decreased with respect to light exposure. This change reflects the microstructure change of polymer chains. As the radiation energy broke the chemical bonds in the polymer backbone, the long aramid chains turned into relatively shorter chains and cross-links formed (Figure 29). The short chains and cross-links tend to form crystalline regions. When a load is applied to the fibres,

the resistance from crystalline regions prevents extension that results a lower elongation at break.

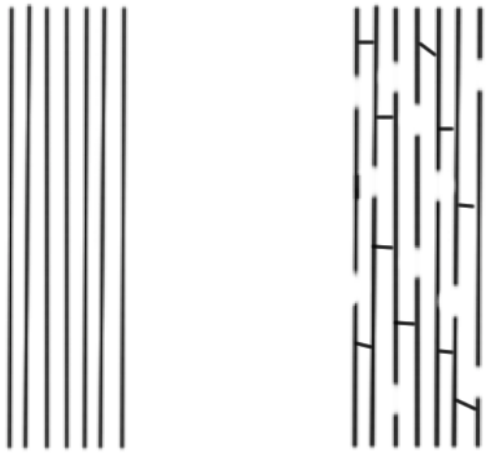

(a) (b)

Figure 29. The model of polymer chains ((a) the ideally perfect long polymer chains arrange parallel, (b) polymer chains after radiation)

The applied TiO_2 film reduced the decrease of elongation at break during the accelerated photodegradation. Table 25 presents the change of elongation at break of fabrics after exposure to 60 AFU and 120 AFU. The elongation of original fabric A decreased 61.8% after exposure to 120 AFU. For the coated fabric A, the elongation decreased 47.7% for low concentration sol-gel coating and 41.7% for high concentration sol-gel coating after exposure to 120 AFU. This also occurred with fabric B and fabric C. This demonstrates that the TiO_2 film on fibre surface inhibited the breaking of polymer chains.

Table 25. Change of elongation at break (%) (n=5) of fabrics after exposure to 60 AFU and 120 AFU

	Light exposure	A (184g/m^2)	B (196g/m^2)	C (255g/m^2)
Original uncoated	0 AFU	57.1%	60.7%	74.2%
	60 AFU	28.1%	30.9%	43.5%
	Change percentage	-50.8%	-49.1%	-41.4%
	120 AFU	21.8%	24.6%	34.9%
	Change percentage	-61.8%	-59.5%	-53.0%
Low concentration	0 AFU	34.4%	36.4%	40.1%
	60 AFU	23.2%	25.5%	29.4%
	Change percentage	-32.6%	-29.9%	-26.7%
	120 AFU	18.0%	20.5%	22.4%
	Change percentage	-47.7%	-43.7%	-44.1%
High concentration	0 AFU	34.3%	32.5%	43.6%
	60 AFU	25.7%	27.6%	32.2%
	Change percentage	-25.1%	-15.1%	-26.1%
	120 AFU	20.0%	21.1%	25.1%
	Change percentage	-41.7%	-35.1%	-42.4%

Change percentage (%) = 100 (elongation at 0 AFU – elongation at 60 or 120 AFU) / elongation at 0 AFU

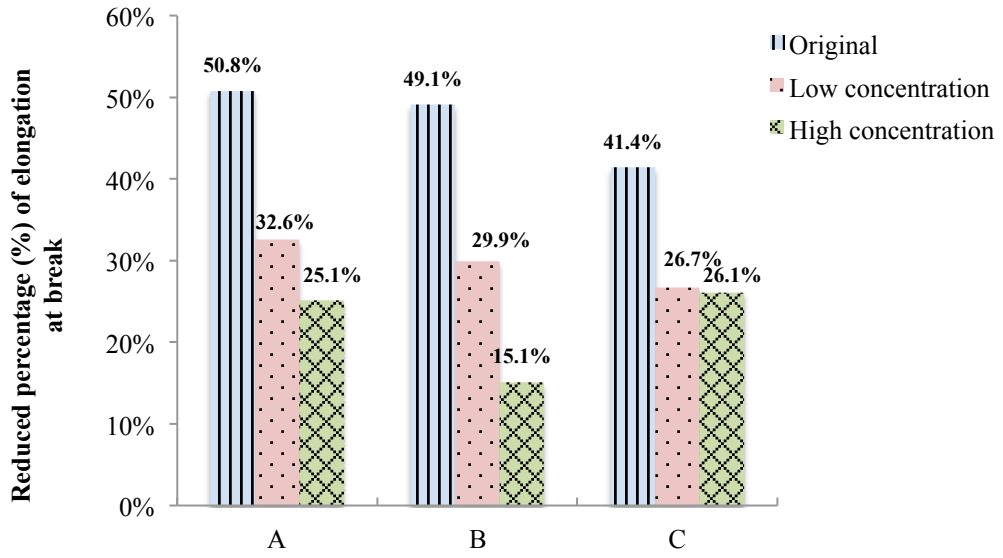

Figure 30. Reduced percentage (%) of elongation at break of fabric A (184g/m^2), B (196g/m^2) and C (255g/m^2) after exposure to 60 AFU

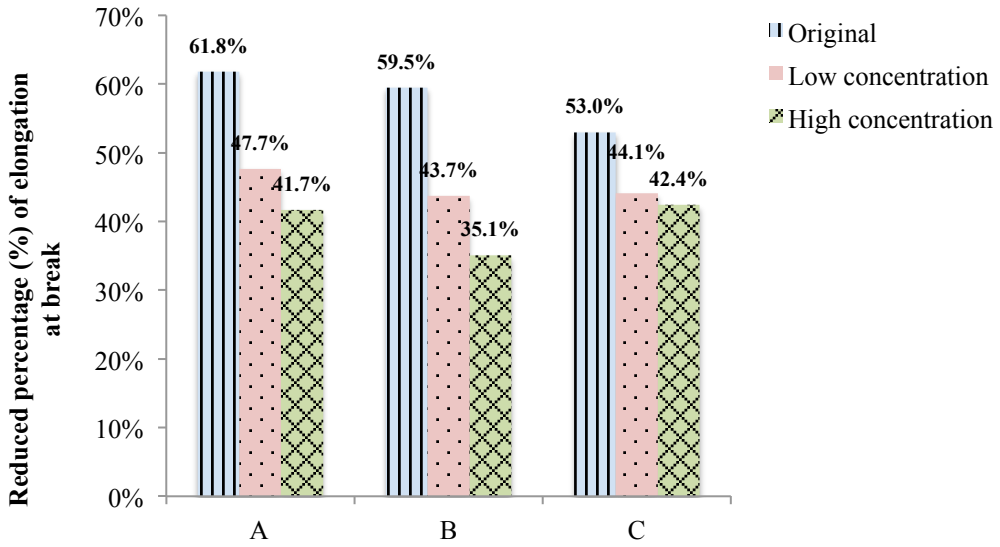

Figure 31. Reduced percentage (%) of elongation at break of fabric A (184g/m^2), B (196g/m^2) and C (255g/m^2) after exposure to 120 AFU

X-Ray photoelectron spectroscopy (XPS) testing

The chemical composition changes of original uncoated and coated fabrics before and after exposure were examined by X-ray photoelectron spectroscopy. The chemical structure of Nomex® includes benzene rings. This unsaturated ring has a greater potential to absorb ultraviolet and visible radiation. According to a study by Carlsson *et al.*, (1978b) of aramid fabric, the absorbed radiation energy from UV and visible light can cause the cleavage of amide linkages (−CO−NH−). Their research also found that carboxylic acid group (−COOH) and nitroso group (−N=O) were formed from the reaction in the presence of oxygen. The C 1*s* spectra of Nomex® fabric were analyzed to present the compositional changes during the exposure. The details are described in Figure 32 to 34.

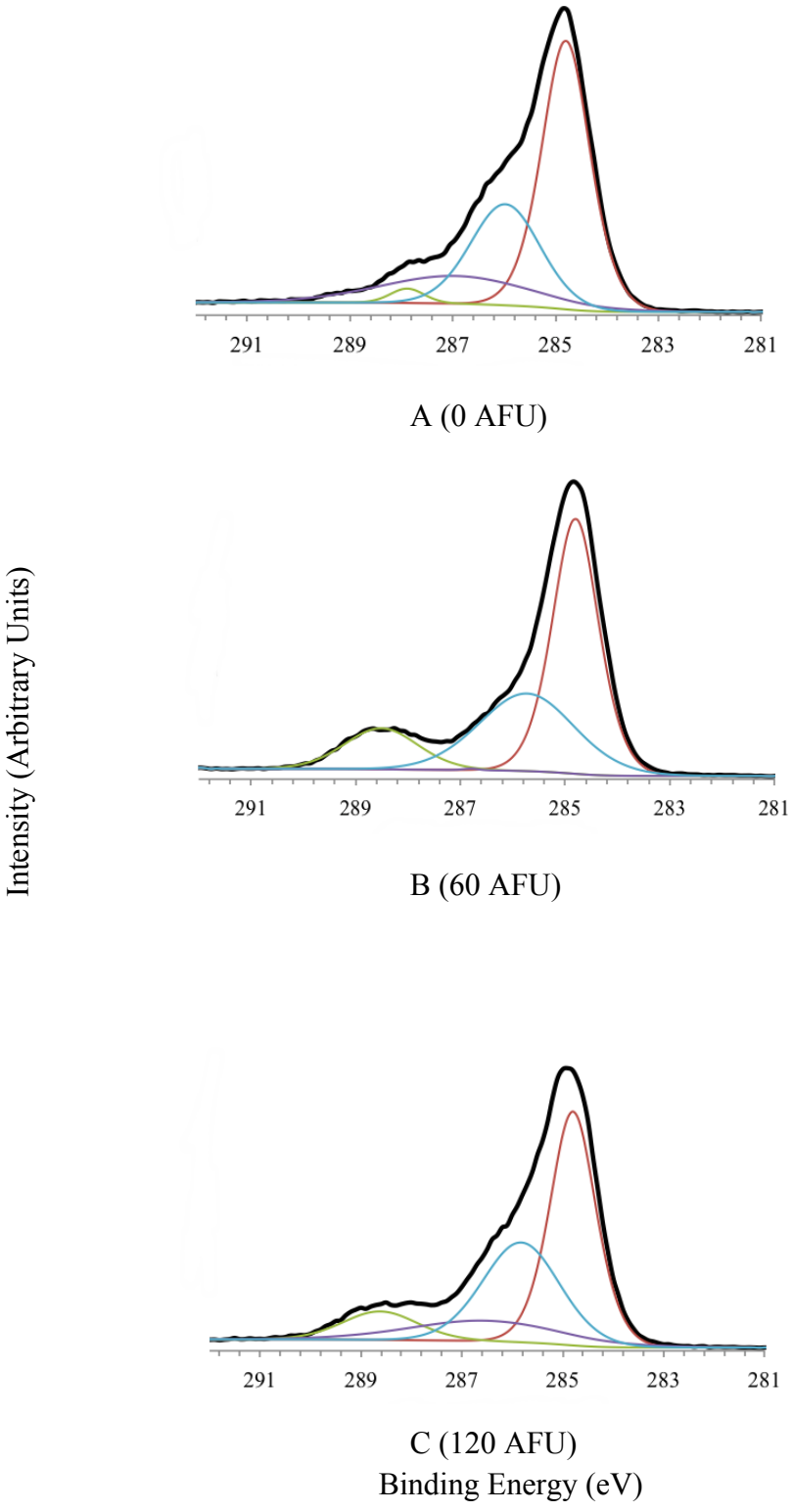

Figure 32. XPS carbon 1*s* spectra of original uncoated Nomex® fabric with exposure of A (0 AFU), B (60 AFU), and C (120 AFU)

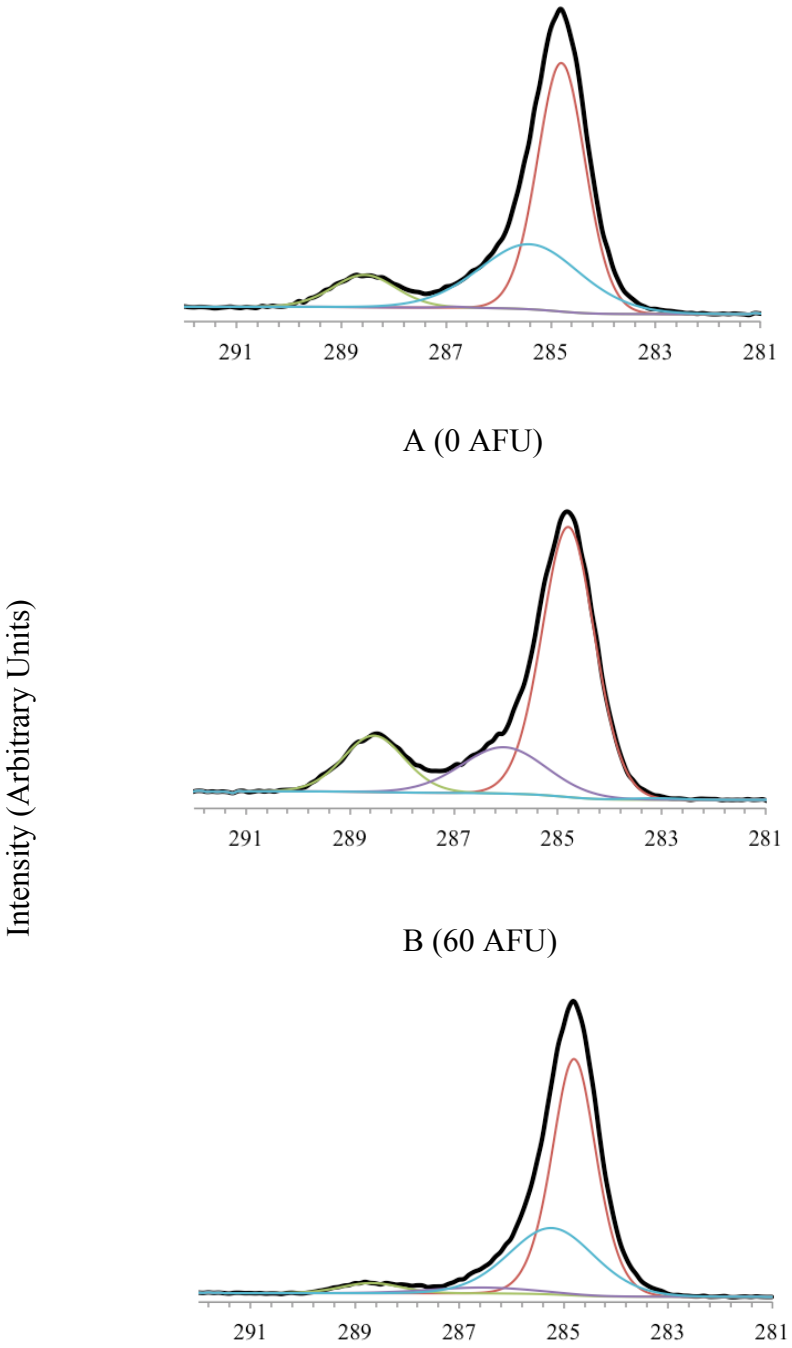

Figure 33. XPS carbon 1*s* spectra of low concentration sol-gel coated Nomex® fabric with exposure of A (0 AFU), B (60 AFU), and C (120 AFU)

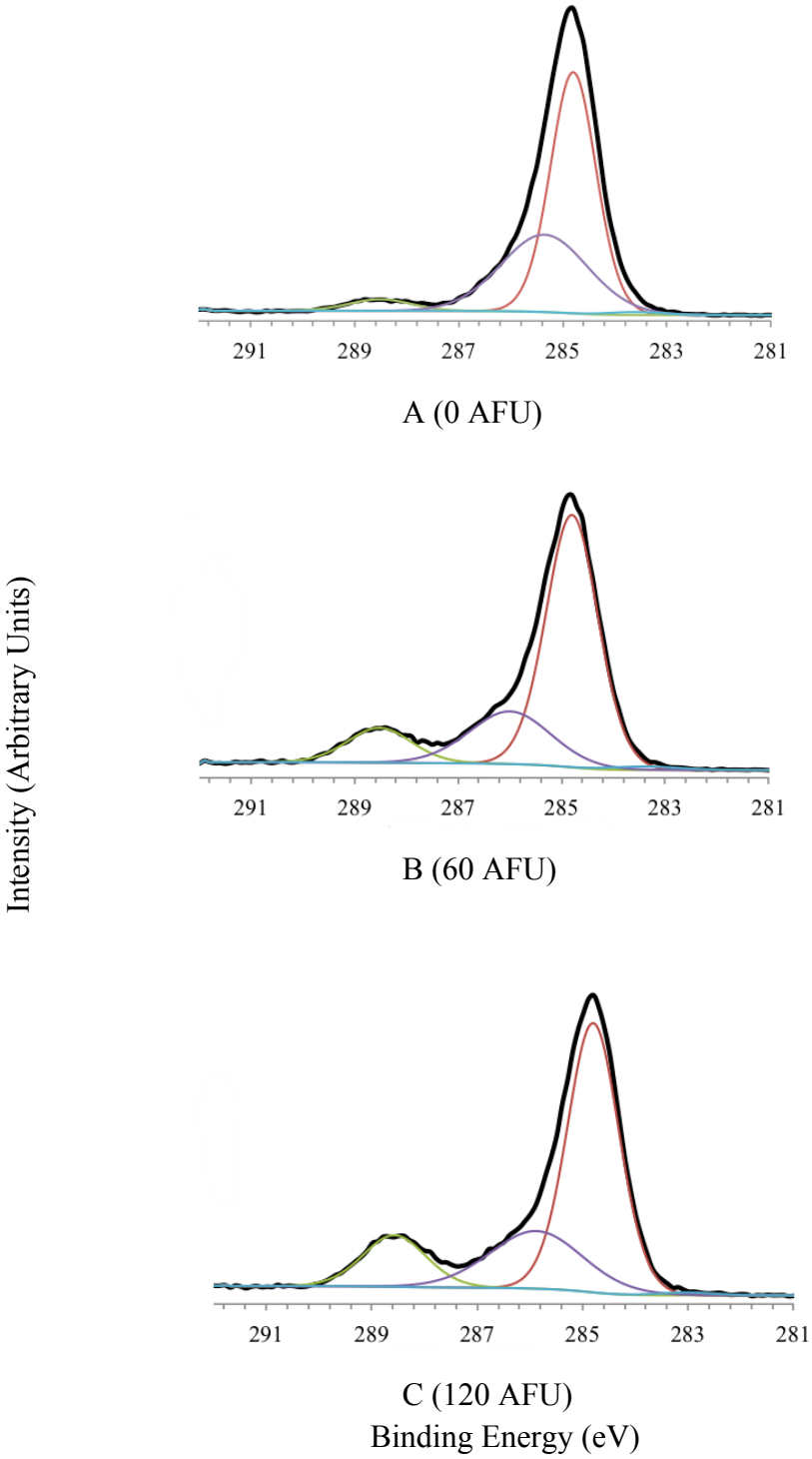

Figure 34. XPS carbon 1*s* spectra of high concentration sol-gel coated Nomex® fabric with exposure of A (0 AFU), B (60 AFU), and C (120 AFU)

The XPS spectra confirmed some of the compositional changes. In the C 1*s* spectra, the intense peak at 284.8 eV presents the carbons in the benzene rings. The photodegradation of the Nomex® fabric caused the amide linkages to split and increased the intensity of C 1*s* peaks at 286.8 eV, presenting the formation of >C=O bond in groups including hydroxyl, ether, or ketone groups (Hamilton *et al.*, 1993). The increasing intensity of C 1*s* peaks at 288.5 eV presents the formation of >C=O bond in carboxylic acid end groups.

The atomic concentration of C 1*s* in various compound state in the Nomex® fabric is given in Table 26. The atomic concentration of C 1*s* in −COOH increased with the light exposure. For original uncoated fabric, the atomic concentration increased by 13.4% after exposure to 120 AFU. For coated fabric, the TiO_2 film slows the change of C 1*s* in –COOH. After exposure to 120 AFU, it increased by 12.5% and 10.5% for low and high concentration sol-gel coating, respectively.

Table 26. C 1*s* changes in original uncoated and coated fabrics

Sample	Atomic concentration (%) of C 1*s*			
	A (C-C)	B (-COOH)	C (C=O)	D (C-H)
Uncoated at 0AFU	53.23	1.95	16.66	28.16
Uncoated at 60AFU	45.99	8.89	12.96	32.16
Uncoated at 120AFU	53.72	15.34	0.1	30.84
Low at 0AFU	61.01	3.38	3.41	32.19
Low at 60AFU	57.89	9.93	0.11	31.98
Low at 120AFU	65.67	15.88	18.09	0.36
High at 0AFU	59.27	3.84	35.98	0.9
High at 60AFU	66.12	11.17	21.5	1.22
High at 120AFU	61.47	14.3	23.54	0.69

Size of TiO_2 nano-sized particle -X ray diffraction (XRD) testing

The size of TiO_2 particles on coated Nomex® fabrics is determined by X ray diffraction (XRD). Samples of fabric C (255g/m^2) coated with both low and high concentration TiO_2 sol solution are selected for XRD testing. The XRD spectra are shown in Figure 35 and 36.

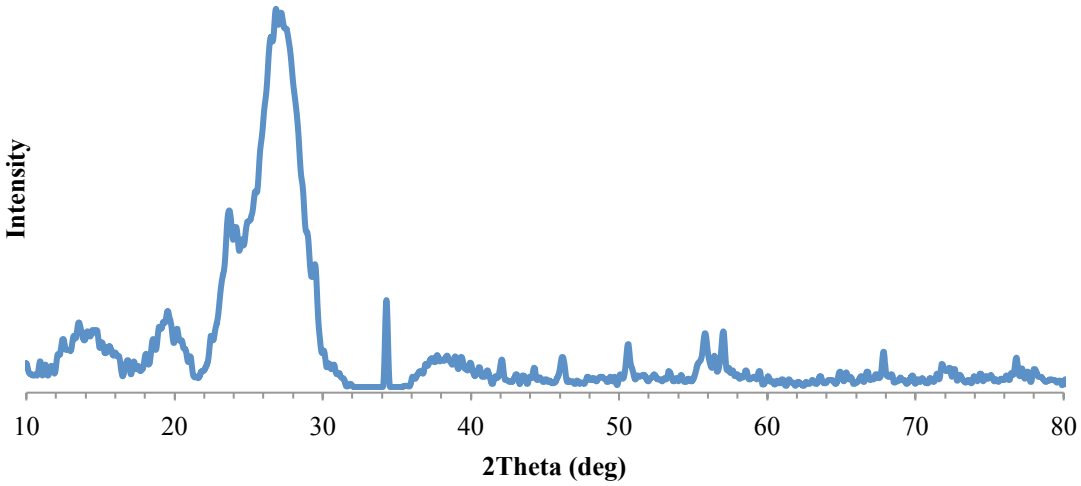

Figure 35. XRD spectrum of TiO_2 particles on Nomex® fabric coated by low concentration sol solution

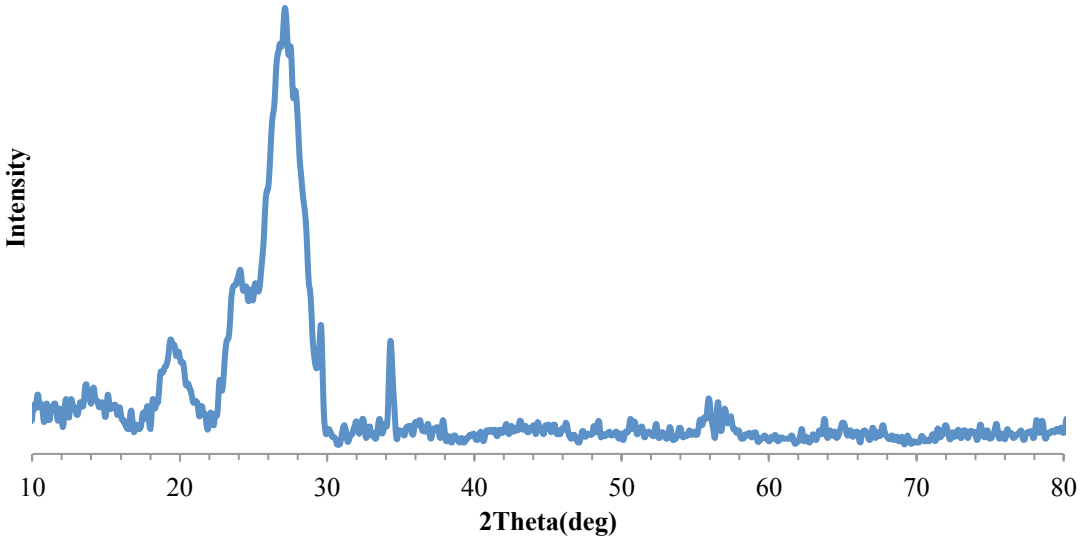

Figure 36. XRD spectrum of TiO_2 particles on Nomex® fabric coated by high concentration sol solution

The weak peak on 29° revealed that anatase TiO_2 particles are formed on coated fabric surface. The average size of the TiO_2 particle is calculated according to Eq(3), where K= 0.9, λ= 1.79026Å and the FWHM and 2θ are given in Table 27.

Table 27. Average size of anatase TiO_2 particle on coated fabric

Concentration of sol solution (mol/L)	FWHM	2θ	Average size of anatase TiO_2 particle (mm)
0.414	0.419	29.4°	22.1
0.827	0.359	29.6°	25.7

Crystalline titanium dioxide can be obtained from amorphous titanium dioxide by heat treatment. Among the three crystalline forms of TiO_2 (rutile, anatase and brookite), rutile TiO_2 has the highest photostability (Yang *et al.*, 2004). In this study, only anatase titanium dioxide was generated on the Nomex® fabric surface by applying the curing parameters in coating treatment. The average size of the anatase titanium dioxide particles is about 22.1 nm and 25.7 nm, respectively.

A nanosol is a colloidal solution of nanometre-sized oxide particles in aqueous or organic solvent (Mahltig & Textor, 2008). In this study, TiO_2 nanosol solution is a colloidal solution of nanometre sized titanium oxide particles in ethanol. Due to the very high surface area of the nanometre sized TiO_2 particles, the sols are not very stable. The TiO_2 particles aggregated as the solvent evaporated, forming a continuous three-dimensional network during the coating process.

Scanning electron microscopy (SEM) testing

The surface changes of original uncoated and coated fabrics were studied by scanning electron microscopy. Figure 37, 38 and 39 show the micrographs of the original uncoated and coated Nomex® fabrics.

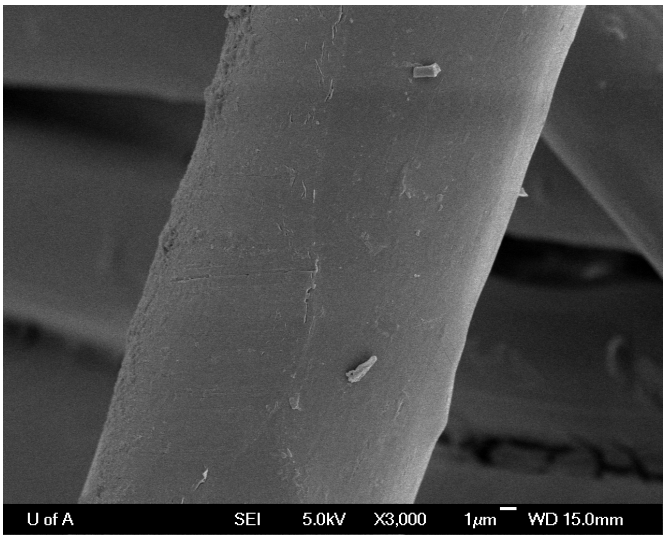

(a)

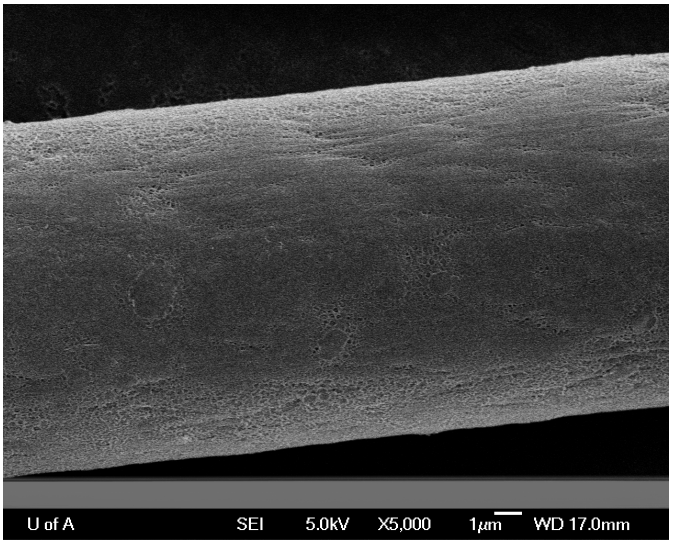

(b)

Figure 37. Fibre from original uncoated Nomex® fabric ((a) 3000 times magnification, (b) 5000 times magnification)

Figure 37 presents the images of single fibre from a Nomex® fabric. Figure 37 (a) shows a smooth surface of original Nomex® fibre under 3000 times magnification. Micrograph with the magnification of 5000 times (Figure 37 (b)) shows longitudinal lines along the fibre surface.

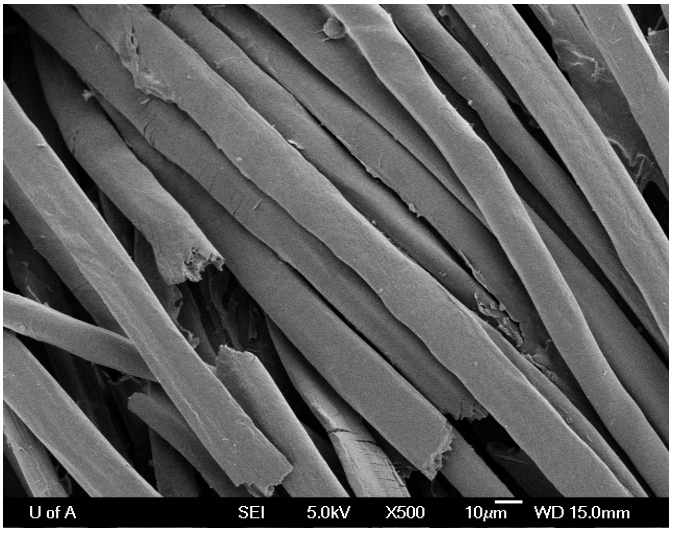

(a)

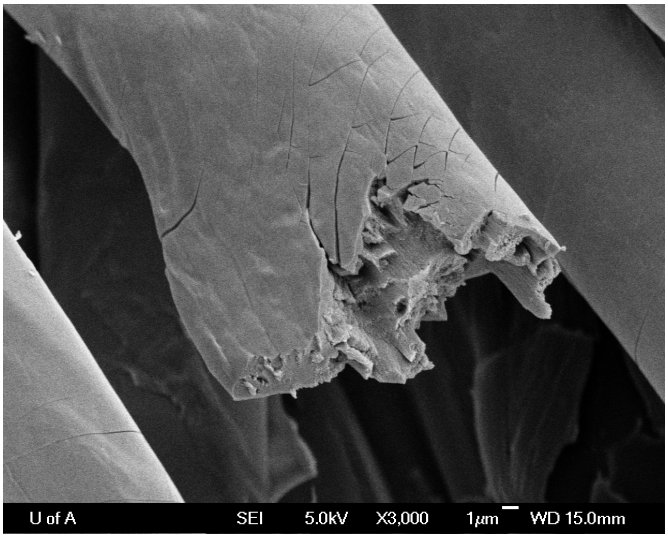

(b)

Figure 38. Photodegraded original Nomex® fibre after tensile breaking

Figure 38 presents the images of photodegraded Nomex® fabric after breaking strength testing. Figure 38(a) shows the fibre fracture ends after the tensile failure in a bundle of fibres. High magnification of a single fibre fracture end shows that the sharp cleavage caused by the brittle failure was consistent with the loss of breaking strength.

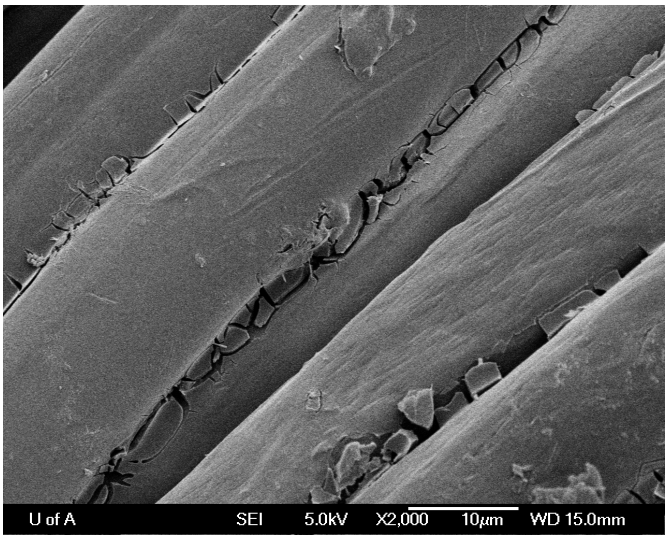
U of A
SEI
5.0kV
X2,000
10μm
WD 15.0mm

(a)

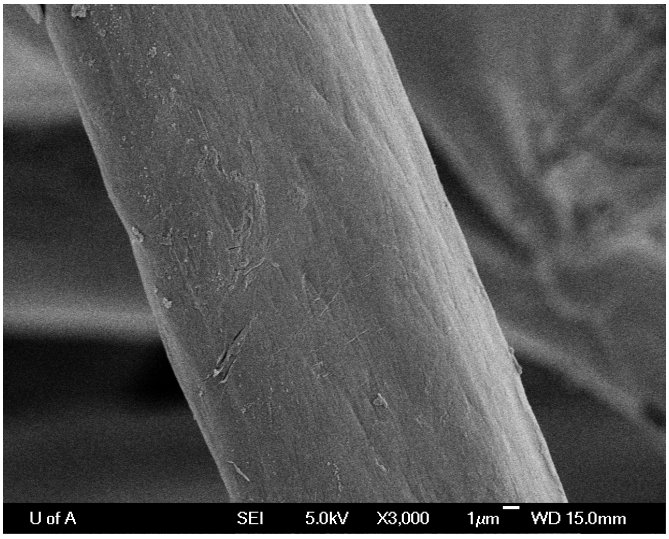
U of A
SEI
5.0kV
X3,000
1μm
WD 15.0mm

(b)

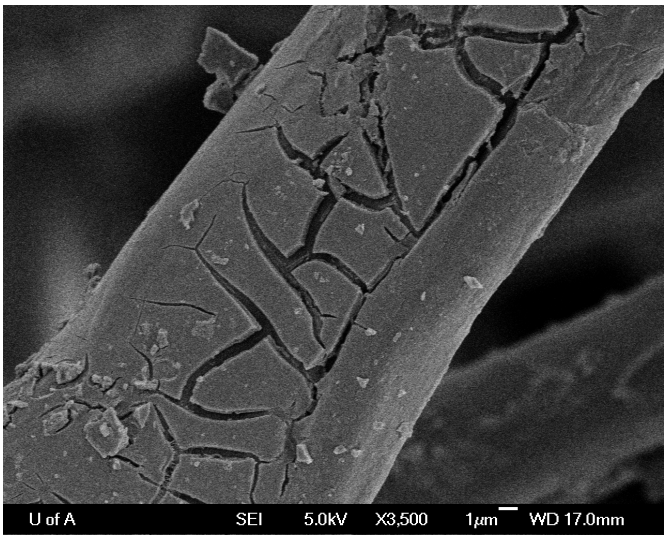

(c)

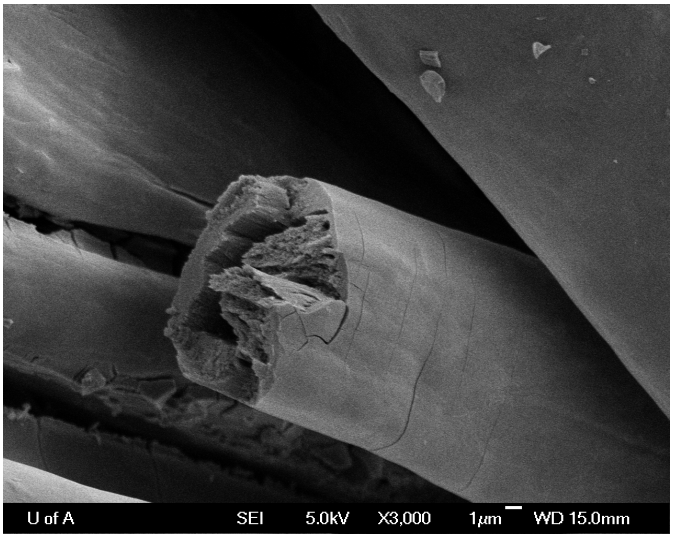

(d)

Figure 39. TiO_2 coated Nomex® fabrics

Figure 39 exhibits the images of coated Nomex® fabric. Figure 39(a) shows the high concentration sol-gel coated fabric B (196g/m^2). Not only the surface of fibres was coated with TiO_2 films, but also the gaps between the fibres were filled with TiO_2 bridges. Figure 39(b) presents a smooth fibre surface from low concentration sol-gel coated fabric C (255g/m^2). However in Figure 39(c), cracks were found on a fibre surface of high concentration sol-gel coated fabric C

(255g/m^2). The cracks were also found on the TiO_2 film formed in the gaps between fibres in Figure 39(a). The cause for these cracks can be explained by the tension generated during the evaporation of solvent in the drying and curing process. During the continuous evaporation of solvent from the gel network, the coating network started to shrink and the tension split the films into cracks. These cracks may lead to ineffectiveness of the TiO_2 coatings. Figure 39(d) shows a breaking fibre from the high concentration sol-gel coated fabric C (255g/m^2) after the photodegradation.

SEM images roughly provided an estimation of the TiO_2 film thickness. The thickness of TiO_2 film showed dependence on the sol solution concentration. The thickness of film generated from the low concentration sol solution ranged from tens of nanometres to 100 nanometre. The thickness of film generated from the high concentration sol solution was thicker than 300 nanometre. The concentration of the sol solution is an approach to control the film thickness. The thickness of TiO_2 film is a critical parameter in protecting the substrate material Nomex® fibre from photodegradation which is largely a surface chemical phenomenon. The depth that the photons penetrate into substrate material determines the degree of photo damages. For systems that principally absorb photons, the Beer-Lambert law considers the relationship between the radiation intensity and the penetration depth (Feller, 1994). According to the Beer-Lambert law, the thickness of ultraviolet absorber film should arrive at an effective thickness in order to protect substrate material underneath.

Additional observations

The color changes of fabrics are observed during the photodegradation experiment and sol-gel coating. In the accelerated photodegradation experiment,

one side of the fabric was exposed to radiation (Figure 12). The color of fabric area exposed to radiation turned from ivory to yellow. The yellow color became darker with a longer light exposure. On the other side of the fabric, this color change was not observed. This phenomenon can be explained by the fact that photodegradation is a chemical reaction on polymer surface. Nomex® fabric formed a thin degraded layer on the fibre surface. This layer can protect the bulk underneath from further degradation (Blais *et al*., 1973; Dupont, 2001). This is further demonstrated by the photodegradation rate presented in Figure 18.

The color changes after the sol-gel coating are also observed. After the high temperature drying and curing, the coated fabrics became brown compared to the original ivory color. Titanium dioxide coating was reported to yield a slight yellow color (Mahltig & Textor, 2008). However, the yield brown color in this study is a sign of the damage from the acid sol solution. As explained in the previous part, the high temperature treatment increased the acidity of the solution on the fabric surface dramatically. Under the high acidity environment, the acid caused hydrolysis of amide linkage and a color change.

Besides the color changes, the hand softness of the fabric was found to decrease after coating. This is because the bridging of the fibres increased the stiffness of the fabric. The bridge may also affect other comfort properties such as air permeability, thermal resistance and moisture resistance.

CHAPTER 5 CONCLUSIONS, IMPLICATIONS, & FUTURE WORK

CONCLUSIONS

The following conclusions apply only to the specific aramid fabrics, sol-gel coating materials and methods, and analytical equipment used in this study. The first objective of this study was to find an effective method to improve the photostability of aramid fabrics. The following conclusions meet this objective:

- The TiO_2 films significantly decelerated the photodegradation rate. The TiO_2 coated fabric exhibits less loss of breaking strength and elongation at break than the original uncoated fabric after the light exposure.
- The tensile properties of original uncoated aramid fabric were reduced after the photodegradation. Breaking strength and elongation at break of fabric were decreased with respect to the light exposure.
- The chemical composition of original uncoated aramid fabric changed after photodegradation. Carboxylic groups were formed as a sign of photo oxidation reaction. For TiO_2 coated fabric, the chemical composition changes also happened, but not as much as the original uncoated one.
- A titanium dioxide sol solution was successfully prepared to achieve a nanometre-sized titanium dioxide particle.
- The nanometre-sized titanium dioxide particles formed a thin film on the surface of aramid fibres and bridged the gaps between the fibres.

The second objective of this study was to investigate the effects of TiO_2 sol-gel coating on aramid fabrics. The following conclusions are made:

- The TiO_2 film increased the total mass of aramid fabric. A higher concentration sol-gel gained a higher add-on weight on aramid fabric; a

loosely woven fabric gained a higher add-on weight.

- The TiO_2 sol gel treatment decreased the initial breaking strength of aramid fabric. The possible causes to this damage were: (1) the structure of aramid fabric changed and the flexibility and movement of fibres were restricted; (2) the acid environment of the sol solution applied during the coating process weakened the aramid fibres that make up the fabric.
- The thickness of the TiO_2 film varied from tens of nanometres to 300 nm. The TiO_2 film formed on the fibre surface and also the gaps between fibres.
- The TiO_2 film blocked the ultraviolet and visible light arriving at the surface of aramid fibres. It inhibited the initiation of photodegradation to some degree.

IMPLICATIONS

Aramid fibre, an important high performance fibre, is widely used in industries, military, aerospace, and protective clothing and so on. The unsaturated structure makes the fibre very vulnerable to ultraviolet and visible light. When the fibre is exposed to ultraviolet and visible light, the photodegradation occurs and causes the loss of tensile properties and changes of the chemical composition of aramid fibre. The loss of tensile properties influences the service of the aramid fibre products. The TiO_2 sol-gel coating approach in this study is an attempt to apply a chemical coating method to improve the photostability of aramid fabric. The whole sol-gel coating process includes the preparation of sol solution, coating and drying. Each step plays an important role in controlling the TiO_2 particle size, film thickness and morphology. The TiO_2 film generated on the aramid fabrics in this study reduced the photodegradation rate of Nomex® fabric. However, the treatment itself lowered the initial breaking strength of fabric.

FUTURE WORK

This research demonstrates the challenges of applying sol-gel coating method on aramid fabric to improve the photostability. Some of the future work is proposed:

- Aramid fibres are only a small part of the high performance fibres. The wide application of high performance fibres makes it necessary to study the photodegradation of other high performance fibres.
- Greige Nomex® fabric was chosen to receive the sol-gel coating in this study. The purpose of using a greige fabric was to avoid the potential influence of finishings on sol-gel coating. The finishings during the product manufacturing may affect the photostability and sol-gel coating. It is interesting to evaluate the influence from finishings. The finished fibres or fabrics should be chosen to receive the photodegradation experiment and sol-gel coating.
- The sol-gel coating itself impaired the initial strength of aramid fabric. This result negatively influences the sol-gel coating effectiveness. The possible causes to this damage were the fabric structure changes and the acid environment of sol solution. The future work will try to find a moderate sol solution formulation and drying parameters to reduce the damage.
- The flame resistance is very important in the application of Nomex®. The impact of TiO_2 film on the flame resistance of Nomex® fabric should be considered as an index to evaluate the coating's performance.
- The abrasion resistance and laundry durability of the TiO_2 film is an essential part of this study. To study the durability of the TiO_2 film may help to understand the interface interactions between the TiO_2 film and the aramid fibre.

- The gaps between fibres filled with TiO_2 bridges would change the comfort properties of the coated fabrics. The comfort properties such as air permeability, thermal resistance and moisture resistance need to be investigated.

REFERENCES

Abidi, N., Hequet, E., Tarimala, S., & Dai, L. L. (2007). Cotton fabric surface modification for improved UV radiation protection using sol-gel process. *Journal of Applied Polymer Science, 104*(1), 111-117.

Afshari, M., Sikkema, D. J., Lee, K., & Bogle, M. (2008). High performance fibres based on rigid and flexible polymers. *Polymer Reviews, 48*(2), 230-274.

American Association of Textile Chemists and Colorists. (2007). *AATCC Test Method 16-2004 Colorfastness to Light.* Research Triangle Park, NC: Author.

American Association of Textile Chemists and Colorists. (2007). *AATCC Test Method 135-2004 Dimensional Changes of Fabrics after Home Laundering*. Research Triangle Park, NC: Author.

American Society for Testing and Materials. (2006). *ASTM F1407 - 99a Standard Test Method for Resistance of Chemical Protective Clothing Materials to Liquid Permeation-Permeation Cup Method.* West Conshohocken, PA:Author

American Society for Testing and Materials. (2008). *ASTM F1930 - 00 Standard Test Method for Evaluation of Flame Resistant Clothing for Protection Against Flash Fire Simulations Using an Instrumented Manikin.* West Conshohocken, PA:Author

Awitor, K. O., Rivaton, A., Gardette, J.-L, Down, A. J., & Johnson, M. B. (2008). Photo-protection and photo-catalytic activity of crystalline anatase titanium dioxide sputter-coated on polymer films. *Thin Solid Films, 516*(8), 2286-2291.

Blais, P., Carlsson, D. J., Parnell, R. D., & Wiles, D. M. (1973). High performance fibres part 2:Limitations:Photo and thermal degradation. *Canadian Textile Journal, 90*(7), 93-96.

Bourbigot, S., & Flambard, X. (2002). Heat resistance and flammability of high performance fibres: A review. *Fire and Materials, 26*(4-5), 155-168.

Bourne, J. K. (2010, October). The Gulf of oil: Is another deepwater disaster

inevitable? National Geographic, 218, 28-53.

Brinker, C. J., & Scherer, G. W. (1990). *Sol-gel science: The physics and chemistry of sol-gel processing*. San Diego: Academic Press, Inc.

Brown, J. R., Browne, N. M., Burchill, P. J., & Egglestone, G. T. (1983). Photochemical aging of Kevlar-49. *Textile Research Journal, 53*(4), 214-219.

Canadian General Standards Board. (1989). *CAN/CGSB-4.2 No. 6-M89/ISO 7211/2:1984 Textile test methods – textiles – woven fabrics – construction – methods of analysis – part 2: Determination of number od threads per unit length*. Ottawa, ON: Author.

Canadian General Standards Board. (2002). *CAN/CGSB-4.2 No. 37-2002 Textile test methods – fabric thickness.* Ottawa, ON: Author.

Canadian General Standards Board. (2004). *CAN/CGSB-4.2 No. 5.1-M90 Textile test methods – unit mass of fabrics.* Ottawa, ON: Author.

Canadian General Standards Board. (2004). *CAN/CGSB-4.2 No. 9.1-M90 Textile test methods – breaking strength of fabrics – strip method – constant-time-to-break principle.* Ottawa, ON: Author.

Carlsson, D. J., Gan, L. H., & Wiles, D. M. (1978a). Photodegradation of aramids .1. irradiation in absence of oxygen. *Journal of Polymer Science Part A-Polymer Chemistry, 16*(9), 2353-2363.

Carlsson, D. J., Gan, L. H., & Wiles, D. M. (1978b). Photodegradation of aramids .2. irradiation in air. *Journal of Polymer Science Part A-Polymer Chemistry, 16*(9), 2365-2376.

Carlsson, D. J., & Wiles, D. M. (1973). High performance fibres part 1: Types, properties and applications. *Canadian Textile Journal, 90*(6), 107-110.

CasaXPS. (2006). Peak fitting in XPS. Retrieved May 17, 2011, from http://www.casaxps.com/help_manual/manual_updates/peak_fitting_in_xps.pdf

Chung, T. S., & Herold, F. K. (1991). High-modulus polyaramide and polybenzimidazole blend fibers. *Polymer Engineering and Science, 31*(21), 1520-1526.

Daoud, W. A., & Xin, J. H. (2004). Low temperature sol-gel processed photocatalytic titania coating. *Journal of Sol-Gel Science and Technology, 29*(1), 25-29.

Davis, R., Chin, J., Lin, C., & Petit, S. (2010). Accelerated weathering of polyaramid and polybenzimidazole firefighter protective clothing fabrics. *Polymer Degradation and Stability, 95*(9), 1642-1654.

Dobashi, Y., & Ohkatsu, Y. (2008). Dependence of ultraviolet absorbers' performance on ultraviolet wavelength. *Polymer Degradation and Stability, 93*(2), 436-447.

Dobashi, Y., Yuyama, T., & Ohkatsu, Y. (2007). Interaction of ultraviolet absorbers. *Polymer Degradation and Stability, 92*(7), 1227-1233.

Dupont. (2001). Technical guide for Nomex® brand fibre. Retrieved January 20 2011,from http://www2.dupont.com/Personal_Protection/en_US/assets/downloads/nomex/Nomex_Techinical_Guide.pdf

Dupont. (2002). Nomex® wash and care guidelines. Retrieved November 11 2010,from http://www.dpp-europe.com/plugins/fckeditor/UserFiles/Nomex%20wash%20&%20care%20guidelines%20Jun%2002%20.pdf

Fechine, G. J. M., Rabello, M. S., & Souto-Maior, R. M. (2002). The effect of ultraviolet stabilizers on the photodegradation of poly(ethylene terephthalate). *Polymer Degradation and Stability, 75*(1), 153-159.

Feldman, D. (2002). Polymer weathering: Photo-oxidation. *Journal of Polymers and the Environment, 10*(4), 163-173

Feller, R. L. (1994). *Accelerated aging:Photochemical and thermal aspects*. Los Angeles: The Getty Conservation Institute.

Fraïsse, F., Kumar, A., Commereuc, S., & Verney, V. (2006). Photo-oxidation of polymers: Validation of oxygen uptake and relationship with extent of hydroperoxidation. *Journal of Applied Polymer Science, 99*(5), 2238-2244.

Fung, W. (2002). *Coated and laminated textiles*. Cambridge, England: CRC Press/Woodhead Publishing.

Gabara, V., Hartzler, J. D., Lee, K.S., Rodini, D. J., & Yang, H. H. (2006).

Aramid fibres. In Lewin, M. (Eds), *Handbook of fibre chemistry, 3rd edition* (pp. 976-1025). Boca Raton, FL: Taylor & Francis Groups

Gijsman, P., Meijers, G., & Vitarelli, G. (1999). Comparison of the UV-degradation chemistry of polypropylene, polyethylene, polyamide 6 and polybutylene terephthalate. *Polymer Degradation and Stability, 65*(3), 433-441.

Grattan, D. W. (1978). The oxidative degradation of organic materials and its importance in deterioration of artifacts. *Journal of the international institute for conservation - Canadian group, 4*(1), 17-26.

Guleryuz, H., Kaus, I., Filiàtre, C., Grande, T., & Einarsrud, M. (2010). Deposition of silica thin films formed by sol-gel method. *Journal of Sol-Gel Science and Technology, 54*(2), 249-257.

Gupta, A. P., Saroop, U. K., & Gupta, V. (2007). Studies on the photo-oxidation of PP and PP/mLLDPE blend systems: Thermal, physicochemical, and mechanical behavior. *Journal of Applied Polymer Science, 106*(2), 917-925.

Hamilton, L. E., Sherwood, P. M. A., & Reagan, B. M. (1993). X-ray photoelectron spectroscopy studies of photochemical changes in high-performance fibers. *Applied Spectroscopy, 47*(2), 139-149.

Hoffmann, K., Laperre, J., Avermaete, A., Altmeyer, P., & Gambichler, T. (2001). Defined UV protection by apparel textiles. *Archives of Dermatology, 137*(8), 1089-1094.

Horta, A., Coca, J., & Díez, F. V. (2003). Degradation kinetics of meta-and para-aromatic polyamides. *Advances in Polymer Technology, 22*(1), 15-21.

Jin, C. Q., Christensen, P. A., Egerton, T. A., Lawson, E. J., & White, J. R. (2006). Rapid measurement of polymer photo-degradation by FTIR spectrometry of evolved carbon dioxide. *Polymer Degradation and Stability, 91*(5), 1086-1096.

Johnson, L. D., Tincher, W. C., & Bach, H. C. (1969). Photodegradative wavelength dependence of thermally resistant organic polymers. *Journal of Applied Polymer Science, 13*(9), 1825-1832.

Kaczmarek, H., Kamińska, A., Kowalonek, J., & Szalla, A. (2000). Accelerated degradation of polymers. *Molecular Crystals and Liquid Crystals, 354*, 1009-1013.

Kalmus, C.E., & Hercules, D. M. (1972). A mechanistic study of photo-Fries rearrangement. *Tetrahedron Letters*, (16), 1575-1577.

Katangur, P., Patra, P. K., & Warner, S. B. (2006). Nanostructured ultraviolet resistant polymer coatings. *Polymer Degradation and Stability, 91*(10), 2437-2442.

Klabunde, K. J., & Richards, R. M. (Eds). (2009). Nanoscale Materials in Chemistry. Hoboken: A John Wiley & Sons. Inc.

Krüger, R., Bockmeyer, M. J., Dutschke, A., & Löbmann, P. C. (2006). Continuous sol-gel coating of ceramic multifilaments: Evaluation of fiber bridging by three-point bending test. *Journal of the American Ceramic Society, 89*(7), 2080-2088.

Li, L., Xing, Y., & Ding, X. (2007). Application of Al^{3+} doped TiO_2 coating on photo-stabilization of aramid fibres. *Proceedings of the 2007 international conference on advanced fibres and polymer materials*, 1,320-322.

Mahltig, B., Haufe, H., & Böttcher, H. (2005). Functionalisation of textiles by inorganic sol-gel coatings. *Journal of Materials Chemistry, 15*(41), 4385-4398.

Mahltig, B., & Textor, T. (2008). *Nanosols and textiles*. Singapore: World Scientific Publishing Co.Pte.Ltd.

MesoLink.org. (2009). *9/11 Ground zero and Mesothelioma*. Retrieved November 11,2010,from http://www.disabled-world.com/health/cancer/mesothelioma/ground-zero.php

Millington, K. R. (2006a). Photoyellowing of wool. part 1: Factors affecting photoyellowing and experimental techniques. *Coloration Technology, 122*(4), 169-186.

Millington, K. R. (2006b). Photoyellowing of wool. part 2: Photoyellowing mechanisms and methods of prevention. *Coloration Technology, 122*(6), 301-316.

Montazer, M., & Pakdel, E. (2010). Reducing photoyellowing of wool using nano TiO_2. *Photochemistry and Photobiology, 86*(2), 255-260.

Morton, M. I. (1974). Below-break tensile behavior of irradiated nylon part III:

Nomex. *Textile Research Journal, 44*(5), 332-335.

National Research Council. (2005). *High-Performance Structural Fibers for Advanced Polymer Matrix Composites.* Retrieved September 9, 2010, from http://www.nap.edu/openbook.php?record_id=11268&page=1

Pandey, J. K., Kim, M. H., Chun, D. M., Lee, C. S., & Ahn, S. H. (2009). Surface modification of polyethylene (PE) by the deposition of titanium dioxide (TiO_2) nanoparticles to enhance the photocatalytic activites. *Surface Review and Letters, 16*(2), 259-263.

Pegoretti, A., & Traina, M. (2009). Liquid crystalline organic fibres and their mechanical behavior. In Bunsell, A. R. (Eds), *Handbook of tensile properties of textile and technical fibres* (pp. 354-426). Cambridge, UK: Woodhead Publishing in association with the Textile Institute

Pospíšil, J., Pilař, J., Billingham, N. C., Marek, A., Horák, Z., & Nešpůrek, S. (2006). Factors affecting accelerated testing of polymer photostability. *Polymer Degradation and Stability, 91*(3), 417-422.

Rabek, J. F. (1990). *Photostabilization of polymers:Principles and applications*. New York: Elsevier Science Publishers Ltd.

Raheel, M. (Ed.). (1994). *Protective clothing systems and materials*. New York: Marcel Dekker, Inc.

Rajakumar, K., Sarasvathy, V., Chelvan, A. T., Chitra, R., & Vijayakumar, C. T. (2009). Natural weathering studies of polypropylene. *Journal of Polymers and the Environment, 17*(3), 191-202.

Rånby, B. G., & Rabek, J.F. (1975). *Photodegradation, photo-oxidation, and photostabilization of polymers; principles and applications*. London, Great Britain: J.W. Arrowsmith Ltd.

Rebouillat, S. (2001). Aramids. In J.W.S. Hearle (Ed.), *High-performance fibres* (pp.23-61). Cambridge England: Woodhead Publishing Ltd.

Singh, B., & Sharma, N. (2008). Mechanistic implications of plastic degradation. *Polymer Degradation and Stability, 93*(3), 561-584.

Sójka-Ledakowicz, J., Lewartowska, J., Kudzin, M., Jesionowski, T., Siwińska-Stefańska, K., & Krysztafkiewicz, A. (2008). Modification of textile materials with micro- and nano-structural metal oxides. *Fibres &*

Textiles in Eastern Europe, 16(5), 112-116.

Su, C., Hong, B. Y., & Tseng, C. M. (2004). Sol-gel preparation and photocatalysis of titanium dioxide. *Catalysis Today, 96*(3), 119-126.

Torikai, A., Shirakawa, H., Nagaya, S., & Fueki, K. (1990). Photodegradation of polyethylene - factors affecting photostability. *Journal of Applied Polymer Science, 40*(9-10), 1637-1646.

Tubbs, M.C., & Daniels, P.N. (Eds). (1991). *Textiles Terms and Definitions.* Manchester, England: Textile Institute

Villar-Rodil, S., Paredes, J. I., Martinez-Alonso, A., & Tascon, J. M. D. (2001). Atomic force microscopy and infrared spectroscopy studies of the thermal degradation of nomex aramid fibers. *Chemistry of Materials, 13*(11), 4297-4304.

Wang, R. H., Xin, J. H., Tao, X. M., & Daoud, W. A. (2004). ZnO nanorods grown on cotton fabrics at low temperature. *Chemical Physics Letters, 398*(1-3), 250-255.

Wei, Q. F., Wang, X. Q., Mather, R. R., & Fotheringham, A. F. (2004). New approaches to characterisation of textile materials using environmental scanning electron microscope. *Fibres & Textiles in Eastern Europe, 12*(2), 79-83.

Wilkie, C. A. (1999). TGA/FTIR: An extremely useful technique for studying polymer degradation. *Polymer Degradation and Stability, 66*(3), 301-306.

Wold, A. (1993). Photocatalytic properties of TiO_2. *Chemistry of Materials, 5*(3), 280-283.

Xin, J. H., Daoud, W. A., & Kong, Y. Y. (2004). A new approach to UV-blocking treatment for cotton fabrics. *Textile Research Journal, 74*(2), 97-100.

Xing, Y., & Ding, X. (2007). UV photo-stabilization of tetrabutyl titanate for aramid fibers via sol-gel surface modification. *Journal of Applied Polymer Science, 103*(5), 3113-3119.

Xing, Y., Yang, X., & Dai, J. (2007). Antimicrobial finishing of cotton textile based on water glass by sol-gel method. *Journal of Sol-Gel Science and Technology, 43*(2), 187-192.

Xue, C., Jia, S., Zhang, J., Tian, L., Chen, H., & Wang, M. (2008). Preparation of

superhydrophobic surfaces on cotton textiles. *Science and Technology of Advanced Materials, 9*(3), 035008.

Yang, H. H. (1989). *Aromatic high strength fibers*. New York: John Wiley & Sons, Inc.

Yang, H. H. (1993). *Kevlar aramid fiber*. Chichester England: John Wiley & Sons, Inc.

Yang, H. Y., Zhu, S. K., & Pan, N. (2004). Studying the mechanisms of titanium dioxide as ultraviolet-blocking additive for films and fabrics by an improved scheme. *Journal of Applied Polymer Science, 92*(5), 3201-3210.

Yang, R., Li, Y., & Yu, J. (2005). Photo-stabilization of linear low density polyethylene by inorganic nano-particles. *Polymer Degradation and Stability, 88*(2), 168-174.

Yang, X. D., & Ding, X. (2006). Prediction of outdoor weathering performance of polypropylene filaments by accelerated weathering tests. *Geotextiles and Geomembranes, 24*(2), 103-109.

Yu, K. F., Zhao, J. Z., Tian, Y. M., Jiang, M., Ding, X. F., Liu, Y. H., & Wang, Z. C. (2005). Preparation of nanosized titanium dioxide from titanium n-butoxide modified with tartaric acid and its influence on the phase transformation. *Materials Letters, 59*(28), 3563-3566.

Zhang, H., Millington, K. R., & Wang, X. (2009). The photostability of wool doped with photocatalytic titanium dioxide nanoparticles. *Polymer Degradation and Stability, 94*(2), 278-283.

Zhang, H., Zhang, J., Chen, J., Hao, X., Wang, S., Feng, X., & Guo, Y. (2006). Effects of solar UV irradiation on the tensile properties and structure of PPTA fiber. *Polymer Degradation and Stability, 91*(11), 2761-2767.

Zhou, W., Reddy, N., & Yang, Y. (2005). Overview of protective clothing. In R.A.Scott (Ed.), *Textiles for protection* (pp.3-30). Cambridge England: Woodhead Publishing Limited.

APPENDIX

Appendix 1.Tensile strength of original fabric A without light exposure

Replicate	Maximum Load (kgf)	Maximum Load (N)	Tensile extension at Maximum load (mm)
1	45.877	449.9	45.60
2	43.407	425.7	40.84
3	46.226	453.3	44.96
4	42.499	416.8	40.30
5	45.453	445.7	42.57
Mean	44.692	438.3	42.85
Standard deviation	1.64	16.11	2.38
CV	0.037	0.037	0.055

Appendix 2. Tensile strength of original fabric A after light exposure to 20 AFU

Replicate	Maximum Load (kgf)	Maximum Load (N)	Tensile extension at Maximum load (mm)
1	37.060	363.4	30.12
2	37.699	369.7	32.93
3	38.158	374.2	34.12
4	37.066	363.5	31.96
5	37.195	364.8	32.17
Mean	37.436	367.1	32.26
Standard deviation	0.48	4.72	1.47
CV	0.013	0.013	0.046

Appendix 3. Tensile strength of original fabric A after light exposure to 40 AFU

Replicate	Maximum Load (kgf)	Maximum Load (N)	Tensile extension at Maximum load (mm)
1	31.201	306.0	25.60
2	30.101	295.2	24.31
3	30.137	295.5	25.00
4	30.803	302.1	25.25
5	29.913	293.3	25.06
Mean	30.431	298.4	25.05
Standard deviation	0.55	5.36	0.47
CV	0.018	0.018	0.019

Appendix 4. Tensile strength of original fabric A after light exposure to 60 AFU

Replicate	Maximum Load (kgf)	Maximum Load (N)	Tensile extension at Maximum load (mm)
1	25.540	250.5	20.50
2	25.302	248.1	20.55
3	26.045	255.4	22.65
4	25.508	250.2	20.60
5	25.843	253.4	21.15
Mean	25.648	251.5	21.09
Standard deviation	0.29	2.88	0.91
CV	0.011	0.011	0.043

Appendix 5. Tensile strength of original fabric A after light exposure to 80 AFU

Replicate	Maximum Load (kgf)	Maximum Load (N)	Tensile extension at Maximum load (mm)
1	22.213	217.8	19.95
2	23.369	229.2	19.45
3	22.841	224.0	20.15
4	21.834	214.1	19.30
5	22.724	222.8	18.85
Mean	22.596	221.6	19.54
Standard deviation	0.59	5.80	0.52
CV	0.026	0.026	0.027

Appendix 6. Tensile strength of original fabric A after light exposure to 120 AFU

Replicate	Maximum Load (kgf)	Maximum Load (N)	Tensile extension at Maximum load (mm)
1	18.363	180.1	16.80
2	17.902	175.6	16.25
3	17.986	176.4	15.75
4	18.638	182.8	16.55
5	19.194	188.2	16.30
Mean	18.417	180.6	16.33
Standard deviation	0.53	5.16	0.39
CV	0.029	0.029	0.024

Appendix 7. Tensile strength of low concentration sol-gel coated fabric A without exposure

Replicate	Maximum Load (kgf)	Maximum Load (N)	Tensile extension at Maximum load (mm)
1	26.395	258.8	25.78
2	26.651	261.4	25.67
3	26.640	261.3	25.67
4	27.265	267.4	26.11
5	26.737	262.2	25.89
Mean	26.738	262.2	25.83
Standard deviation	0.32	3.15	0.18
CV	0.012	0.012	0.007

Appendix 8. Tensile strength of low concentration sol-gel coated fabric A after light exposure to 20 AFU

Replicate	Maximum Load (kgf)	Maximum Load (N)	Tensile extension at Maximum load (mm)
1	25.088	246.0	24.15
2	25.099	246.1	23.75
3	24.955	244.7	24.28
4	23.874	234.1	23.76
5	23.459	230.1	23.80
Mean	24.495	240.2	23.95
Standard deviation	0.77	7.58	0.25
CV	0.031	0.032	0.010

Appendix 9. Tensile strength of low concentration sol-gel coated fabric A after light exposure to 40 AFU

Replicate	Maximum Load (kgf)	Maximum Load (N)	Tensile extension at Maximum load (mm)
1	21.146	207.4	18.55
2	19.400	190.3	17.55
3	20.117	197.3	17.67
4	20.203	198.1	18.17
5	21.042	206.4	19.50
Mean	20.381	199.9	18.29
Standard deviation	0.72	7.08	0.79
CV	0.035	0.035	0.043

Appendix 10. Tensile strength of low concentration sol-gel coated fabric A after light exposure to 60 AFU

Replicate	Maximum Load (kgf)	Maximum Load (N)	Tensile extension at Maximum load (mm)
1	19.064	187.0	16.10
2	20.008	196.2	18.30
3	20.498	201.0	18.35
4	19.440	190.6	17.35
5	18.423	180.7	16.75
Mean	19.487	191.1	17.37
Standard deviation	0.81	7.91	0.98
CV	0.042	0.041	0.056

Appendix 11. Tensile strength of low concentration sol-gel coated fabric A after light exposure to 80 AFU

Replicate	Maximum Load (kgf)	Maximum Load (N)	Tensile extension at Maximum load (mm)
1	16.780	164.6	15.20
2	16.179	158.7	14.70
3	17.051	167.2	14.90
4	16.424	161.1	14.40
5	16.173	158.6	15.00
Mean	16.521	162.0	14.84
Standard deviation	0.39	3.78	0.30
CV	0.024	0.023	0.020

Appendix 12. Tensile strength of low concentration sol-gel coated fabric A after light exposure to 120 AFU

Replicate	Maximum Load (kgf)	Maximum Load (N)	Tensile extension at Maximum load (mm)
1	14.781	144.9	13.75
2	14.554	142.7	14.20
3	14.144	138.7	13.00
4	14.258	139.8	13.40
5	14.436	141.6	13.05
Mean	14.435	141.6	13.48
Standard deviation	0.25	2.45	0.50
CV	0.017	0.017	0.037

Appendix 13. Tensile strength of high concentration sol-gel coated fabric A without exposure

Replicate	Maximum Load (kgf)	Maximum Load (N)	Tensile extension at Maximum load (mm)
1	27.887	273.5	25.46
2	28.577	280.2	25.89
3	27.788	272.5	25.13
4	28.179	276.3	25.78
5	28.721	281.7	26.43
Mean	28.230	276.8	25.74
Standard deviation	0.41	4.03	0.49
CV	0.015	0.015	0.019

Appendix 14. Tensile strength of high concentration sol-gel coated fabric A after light exposure to 20 AFU

Replicate	Maximum Load (kgf)	Maximum Load (N)	Tensile extension at Maximum load (mm)
1	24.140	236.7	22.20
2	25.112	246.3	22.80
3	24.603	241.3	22.75
4	25.430	249.4	24.10
5	25.030	245.5	22.30
Mean	24.863	243.8	22.83
Standard deviation	0.50	4.91	0.76
CV	0.020	0.020	0.033

Appendix 15. Tensile strength of high concentration sol-gel coated fabric A after light exposure to 40 AFU

Replicate	Maximum Load (kgf)	Maximum Load (N)	Tensile extension at Maximum load (mm)
1	23.313	228.6	20.75
2	22.533	221.0	20.20
3	22.955	225.1	20.65
4	22.481	220.5	19.70
5	22.775	223.4	20.45
Mean	22.811	223.7	20.35
Standard deviation	0.34	3.33	0.42
CV	0.015	0.015	0.021

Appendix 16. Tensile strength of high concentration sol-gel coated fabric A after light exposure to 60 AFU

Replicate	Maximum Load (kgf)	Maximum Load (N)	Tensile extension at Maximum load (mm)
1	20.628	202.3	18.95
2	21.369	209.6	19.35
3	22.131	217.0	19.85
4	21.611	211.9	19.35
5	21.301	208.9	18.80
Mean	21.408	209.9	19.26
Standard deviation	0.54	5.34	0.41
CV	0.025	0.025	0.021

Appendix 17. Tensile strength of high concentration sol-gel coated fabric A after light exposure to 80 AFU

Replicate	Maximum Load (kgf)	Maximum Load (N)	Tensile extension at Maximum load (mm)
1	17.767	174.2	16.25
2	19.863	194.8	17.15
3	19.112	187.4	17.20
4	19.400	190.3	17.25
5	18.760	184.0	17.15
Mean	18.980	186.1	17.00
Standard deviation	0.79	7.74	0.42
CV	0.042	0.042	0.025

Appendix 18. Tensile strength of high concentration sol-gel coated fabric A after light exposure to 120 AFU

Replicate	Maximum Load (kgf)	Maximum Load (N)	Tensile extension at Maximum load (mm)
1	16.092	157.8	14.55
2	16.749	164.3	15.30
3	16.352	160.4	15.30
4	16.536	162.2	14.85
5	15.372	150.7	15.10
Mean	16.220	159.1	15.02
Standard deviation	0.53	5.22	0.32
CV	0.033	0.033	0.021

Appendix 19. Tensile strength of original fabric B without light exposure

Replicate	Maximum Load (kgf)	Maximum Load (N)	Tensile extension at Maximum load (mm)
1	57.783	566.7	44.30
2	57.641	565.3	43.40
3	59.060	579.2	45.27
4	62.876	616.6	47.60
5	60.557	593.9	47.13
Mean	59.583	584.3	45.54
Standard deviation	2.18	21.41	1.80
CV	0.037	0.037	0.040

Appendix 20. Tensile strength of original fabric B after light exposure to 20 AFU

Replicate	Maximum Load (kgf)	Maximum Load (N)	Tensile extension at Maximum load (mm)
1	50.482	495.1	33.50
2	48.331	474.0	33.90
3	51.244	502.5	35.47
4	49.936	489.7	32.63
5	49.401	484.5	33.98
Mean	49.879	489.1	33.90
Standard deviation	1.10	10.80	1.03
CV	0.022	0.022	0.030

Appendix 21. Tensile strength of original fabric B after light exposure to 40 AFU

Replicate	Maximum Load (kgf)	Maximum Load (N)	Tensile extension at Maximum load (mm)
1	40.400	396.2	28.85
2	38.780	380.3	25.10
3	40.385	396.0	28.60
4	39.964	391.9	26.60
5	38.890	381.4	25.30
Mean	39.684	389.2	26.89
Standard deviation	0.80	7.80	1.77
CV	0.020	0.020	0.066

Appendix 22. Tensile strength of original fabric B after light exposure to 60 AFU

Replicate	Maximum Load (kgf)	Maximum Load (N)	Tensile extension at Maximum load (mm)
1	34.973	343.0	23.55
2	35.069	343.9	22.65
3	35.217	345.4	24.05
4	33.573	329.2	22.00
5	35.936	352.4	23.50
Mean	34.954	342.8	23.15
Standard deviation	0.86	8.43	0.82
CV	0.025	0.025	0.035

Appendix 23. Tensile strength of original fabric B after light exposure to 80 AFU

Replicate	Maximum Load (kgf)	Maximum Load (N)	Tensile extension at Maximum load (mm)
1	30.566	299.7	20.75
2	30.144	295.6	20.25
3	30.161	295.8	21.30
4	30.267	296.8	20.25
5	30.950	303.5	20.60
Mean	30.418	298.3	20.63
Standard deviation	0.34	3.35	0.43
CV	0.011	0.011	0.021

Appendix 24. Tensile strength of original fabric B after light exposure to 120 AFU

Replicate	Maximum Load (kgf)	Maximum Load (N)	Tensile extension at Maximum load (mm)
1	25.573	250.8	18.30
2	24.793	243.1	18.40
3	25.116	246.3	18.20
4	25.502	250.1	18.80
5	26.084	255.8	18.70
Mean	25.414	249.2	18.48
Standard deviation	0.49	4.80	0.26
CV	0.019	0.019	0.014

Appendix 25. Tensile strength of low concentration sol-gel coated fabric B without exposure

Replicate	Maximum Load (kgf)	Maximum Load (N)	Tensile extension at Maximum load (mm)
1	38.003	372.7	27.77
2	39.204	384.5	27.30
3	38.926	381.7	28.82
4	37.972	372.4	26.48
5	37.992	372.6	26.13
Mean	38.419	376.8	27.30
Standard deviation	0.60	5.86	1.07
CV	0.016	0.016	0.039

Appendix 26. Tensile strength of low concentration sol-gel coated fabric B after light exposure to 20 AFU

Replicate	Maximum Load (kgf)	Maximum Load (N)	Tensile extension at Maximum load (mm)
1	35.616	349.3	26.30
2	35.365	346.8	26.33
3	35.016	343.4	25.53
4	34.410	337.4	24.87
5	34.570	339.0	25.07
Mean	34.995	343.2	25.62
Standard deviation	0.51	5.02	0.68
CV	0.015	0.015	0.027

Appendix 27. Tensile strength of low concentration sol-gel coated fabric B after light exposure to 40 AFU

Replicate	Maximum Load (kgf)	Maximum Load (N)	Tensile extension at Maximum load (mm)
1	30.303	297.2	22.00
2	31.418	308.1	21.15
3	31.806	311.9	22.50
4	30.326	297.4	20.60
5	31.124	305.2	22.40
Mean	30.995	304.0	21.73
Standard deviation	0.67	6.54	0.83
CV	0.022	0.022	0.038

Appendix 28. Tensile strength of low concentration sol-gel coated fabric B after light exposure to 60 AFU

Replicate	Maximum Load (kgf)	Maximum Load (N)	Tensile extension at Maximum load (mm)
1	27.884	273.4	18.35
2	27.827	272.9	19.40
3	27.947	274.1	19.50
4	27.343	268.1	18.65
5	28.635	280.8	19.90
Mean	27.927	273.9	19.16
Standard deviation	0.46	4.53	0.64
CV	0.016	0.017	0.033

Appendix 29. Tensile strength of low concentration sol-gel coated fabric B after light exposure to 80 AFU

Replicate	Maximum Load (kgf)	Maximum Load (N)	Tensile extension at Maximum load (mm)
1	24.344	238.7	16.90
2	26.558	260.4	18.10
3	25.709	252.1	17.60
4	25.698	252.0	18.05
5	25.440	249.5	17.55
Mean	25.550	250.6	17.64
Standard deviation	0.80	7.80	0.48
CV	0.031	0.031	0.027

Appendix 30. Tensile strength of low concentration sol-gel coated fabric B after light exposure to 120 AFU

Replicate	Maximum Load (kgf)	Maximum Load (N)	Tensile extension at Maximum load (mm)
1	23.230	227.8	16.45
2	23.036	225.9	16.35
3	21.628	212.1	15.10
4	20.548	201.5	13.90
5	22.171	217.4	14.90
Mean	22.123	216.9	15.34
Standard deviation	1.09	10.73	1.07
CV	0.049	0.049	0.070

Appendix 31. Tensile strength of high concentration sol-gel coated fabric B without exposure

Replicate	Maximum Load (kgf)	Maximum Load (N)	Tensile extension at Maximum load (mm)
1	34.621	339.5	25.67
2	32.966	323.3	23.33
3	33.673	330.2	23.80
4	33.588	329.4	25.32
5	33.228	325.9	23.92
Mean	33.615	329.7	24.41
Standard deviation	0.63	6.18	1.02
CV	0.019	0.019	0.042

Appendix 32. Tensile strength of high concentration sol-gel coated fabric B after light exposure to 20 AFU

Replicate	Maximum Load (kgf)	Maximum Load (N)	Tensile extension at Maximum load (mm)
1	29.327	287.6	21.40
2	29.801	292.2	21.45
3	29.822	292.5	21.65
4	29.580	290.1	21.10
5	28.819	282.6	21.05
Mean	29.470	289.0	21.33
Standard deviation	0.42	4.07	0.25
CV	0.014	0.014	0.012

Appendix 33. Tensile strength of high concentration sol-gel coated fabric B after light exposure to 40 AFU

Replicate	Maximum Load (kgf)	Maximum Load (N)	Tensile extension at Maximum load (mm)
1	29.801	292.2	22.05
2	29.704	291.3	21.80
3	28.985	284.2	22.15
4	29.883	293.1	22.80
5	28.363	278.2	20.90
Mean	29.347	287.8	21.94
Standard deviation	0.66	6.43	0.69
CV	0.022	0.022	0.031

Appendix 34. Tensile strength of high concentration sol-gel coated fabric B after light exposure to 60 AFU

Replicate	Maximum Load (kgf)	Maximum Load (N)	Tensile extension at Maximum load (mm)
1	27.906	273.7	20.70
2	27.444	269.1	20.40
3	27.799	272.6	21.05
4	28.049	275.1	20.70
5	27.683	271.5	20.55
Mean	27.776	272.4	20.68
Standard deviation	0.23	2.25	0.24
CV	0.008	0.008	0.017

Appendix 35. Tensile strength of high concentration sol-gel coated fabric B after light exposure to 80 AFU

Replicate	Maximum Load (kgf)	Maximum Load (N)	Tensile extension at Maximum load (mm)
1	24.000	235.4	18.00
2	24.047	235.8	17.25
3	24.042	235.8	17.85
4	24.121	236.5	18.15
5	24.920	244.4	18.10
Mean	24.226	237.6	17.87
Standard deviation	0.39	3.83	0.37
CV	0.016	0.016	0.021

Appendix 36. Tensile strength of high concentration sol-gel coated fabric B after light exposure to 120 AFU

Replicate	Maximum Load (kgf)	Maximum Load (N)	Tensile extension at Maximum load (mm)
1	21.335	209.2	15.65
2	20.589	201.9	16.15
3	20.073	196.8	15.40
4	20.377	199.8	15.80
5	20.672	202.7	16.15
Mean	20.609	202.1	15.83
Standard deviation	0.47	4.58	0.33
CV	0.023	0.023	0.021

Appendix 37. Tensile strength of original fabric C without light exposure

Replicate	Maximum Load (kgf)	Maximum Load (N)	Tensile extension at Maximum load (mm)
1	59.036	578.9	57.87
2	58.426	573.0	56.00
3	58.160	570.4	54.93
4	56.208	551.2	52.80
5	56.580	554.9	56.53
Mean	57.682	565.7	55.63
Standard deviation	1.23	12.01	1.90
CV	0.021	0.021	0.034

Appendix 38. Tensile strength of original fabric C after light exposure to 20 AFU

Replicate	Maximum Load (kgf)	Maximum Load (N)	Tensile extension at Maximum load (mm)
1	47.083	461.7	43.58
2	47.227	463.1	44.25
3	50.227	492.6	46.08
4	50.670	496.9	45.85
5	49.586	486.3	44.92
Mean	48.959	480.1	44.93
Standard deviation	1.69	16.59	1.06
CV	0.035	0.035	0.024

Appendix 39. Tensile strength of original fabric C after light exposure to 40 AFU

Replicate	Maximum Load (kgf)	Maximum Load (N)	Tensile extension at Maximum load (mm)
1	38.741	379.9	35.50
2	40.545	397.6	37.77
3	39.406	386.4	37.77
4	39.255	385.0	35.75
5	40.879	400.9	37.95
Mean	39.765	390.0	36.95
Standard deviation	0.91	8.89	1.21
CV	0.023	0.023	0.033

Appendix 40. Tensile strength of original fabric C after light exposure to 60 AFU

Replicate	Maximum Load (kgf)	Maximum Load (N)	Tensile extension at Maximum load (mm)
1	35.376	346.9	33.95
2	33.121	324.8	31.80
3	35.564	348.8	32.55
4	34.114	334.5	32.48
5	35.234	345.5	32.33
Mean	34.682	340.1	32.62
Standard deviation	1.04	10.20	0.80
CV	0.030	0.030	0.025

Appendix 41. Tensile strength of original fabric C after light exposure to 80 AFU

Replicate	Maximum Load (kgf)	Maximum Load (N)	Tensile extension at Maximum load (mm)
1	30.364	297.8	29.60
2	30.263	296.8	28.43
3	30.347	297.6	29.25
4	30.486	299.0	28.50
5	30.386	298.0	29.55
Mean	30.369	297.8	29.07
Standard deviation	0.08	0.79	0.57
CV	0.003	0.003	0.020

Appendix 42. Tensile strength of original fabric C after light exposure to 120 AFU

Replicate	Maximum Load (kgf)	Maximum Load (N)	Tensile extension at Maximum load (mm)
1	24.638	241.6	26.45
2	24.321	238.5	25.55
3	25.227	247.4	26.95
4	24.098	236.3	25.65
5	24.490	240.2	26.35
Mean	24.555	240.8	26.19
Standard deviation	0.43	4.18	0.59
CV	0.018	0.018	0.023

Appendix 43. Tensile strength of low concentration sol-gel coated fabric C without exposure

Replicate	Maximum Load (kgf)	Maximum Load (N)	Tensile extension at Maximum load (mm)
1	32.392	317.7	31.73
2	30.866	302.7	27.47
3	32.139	315.2	30.13
4	32.131	315.1	29.73
5	33.348	327.0	31.20
Mean	32.175	315.5	30.05
Standard deviation	0.89	8.69	1.65
CV	0.028	0.028	0.055

Appendix 44. Tensile strength of low concentration sol-gel coated fabric C after light exposure to 20 AFU

Replicate	Maximum Load (kgf)	Maximum Load (N)	Tensile extension at Maximum load (mm)
1	26.971	264.5	26.55
2	26.883	263.6	26.20
3	28.226	276.8	27.65
4	27.258	267.3	26.25
5	26.946	264.3	26.15
Mean	27.257	267.3	26.56
Standard deviation	0.56	5.50	0.63
CV	0.021	0.021	0.024

Appendix 45. Tensile strength of low concentration sol-gel coated fabric C after light exposure to 40 AFU

Replicate	Maximum Load (kgf)	Maximum Load (N)	Tensile extension at Maximum load (mm)
1	24.582	241.1	22.70
2	24.127	236.6	22.15
3	24.469	240.0	22.45
4	24.931	244.5	23.80
5	24.897	244.2	23.55
Mean	24.601	241.3	22.93
Standard deviation	0.33	3.25	0.71
CV	0.013	0.013	0.031

Appendix 46. Tensile strength of low concentration sol-gel coated fabric C after light exposure to 60 AFU

Replicate	Maximum Load (kgf)	Maximum Load (N)	Tensile extension at Maximum load (mm)
1	23.594	231.4	22.15
2	22.977	225.3	21.75
3	23.357	229.1	22.60
4	23.572	231.2	21.60
5	23.248	228.0	22.20
Mean	23.350	229.0	22.06
Standard deviation	0.25	2.49	0.40
CV	0.011	0.011	0.018

Appendix 47. Tensile strength of low concentration sol-gel coated fabric C after light exposure to 80 AFU

Replicate	Maximum Load (kgf)	Maximum Load (N)	Tensile extension at Maximum load (mm)
1	20.874	204.7	19.35
2	20.577	201.8	18.80
3	20.795	203.9	18.95
4	20.229	198.4	18.80
5	20.579	201.8	18.55
Mean	20.611	202.1	18.89
Standard deviation	0.25	2.46	0.29
CV	0.012	0.012	0.015

Appendix 48. Tensile strength of low concentration sol-gel coated fabric C after light exposure to 120 AFU

Replicate	Maximum Load (kgf)	Maximum Load (N)	Tensile extension at Maximum load (mm)
1	18.393	180.4	17.10
2	18.253	179.0	16.65
3	17.961	176.1	16.75
4	17.656	173.1	16.55
5	17.942	176.0	16.85
Mean	18.041	176.9	16.78
Standard deviation	0.29	2.83	0.21
CV	0.016	0.016	0.013

Appendix 49. Tensile strength of high concentration sol-gel coated fabric C without light exposure

Replicate	Maximum Load (kgf)	Maximum Load (N)	Tensile extension at Maximum load (mm)
1	34.302	336.4	32.05
2	34.409	337.4	32.48
3	34.153	334.9	33.30
4	34.096	334.4	32.63
5	35.017	343.4	33.00
Mean	34.395	337.3	32.69
Standard deviation	0.37	3.61	0.48
CV	0.011	0.011	0.015

Appendix 50. Tensile strength of high concentration sol-gel coated fabric C after light exposure to 20 AFU

Replicate	Maximum Load (kgf)	Maximum Load (N)	Tensile extension at Maximum load (mm)
1	30.867	302.7	29.50
2	31.180	305.8	29.25
3	32.404	317.8	30.30
4	31.380	307.7	30.23
5	31.538	309.3	29.63
Mean	31.474	308.7	29.78
Standard deviation	0.58	5.66	0.46
CV	0.018	0.018	0.015

Appendix 51. Tensile strength of high concentration sol-gel coated fabric C after light exposure to 40 AFU

Replicate	Maximum Load (kgf)	Maximum Load (N)	Tensile extension at Maximum load (mm)
1	28.741	281.9	27.20
2	28.263	277.2	25.85
3	27.349	268.2	25.20
4	27.872	273.3	26.75
5	27.930	273.9	27.50
Mean	28.031	274.9	26.50
Standard deviation	0.51	5.05	0.96
CV	0.018	0.018	0.036

Appendix 52. Tensile strength of high concentration sol-gel coated fabric C after light exposure to 60 AFU

Replicate	Maximum Load (kgf)	Maximum Load (N)	Tensile extension at Maximum load (mm)
1	26.750	262.3	24.20
2	26.301	257.9	23.35
3	26.220	257.1	23.80
4	25.782	252.8	24.20
5	27.029	265.1	25.05
Mean	26.416	259.1	24.12
Standard deviation	0.49	4.76	0.63
CV	0.019	0.018	0.026

Appendix 53. Tensile strength of high concentration sol-gel coated fabric C after light exposure to 80 AFU

Replicate	Maximum Load (kgf)	Maximum Load (N)	Tensile extension at Maximum load (mm)
1	23.654	232.0	22.95
2	23.807	233.5	22.00
3	24.432	239.6	22.15
4	24.152	236.9	22.10
5	23.435	229.8	21.60
Mean	23.896	234.3	22.16
Standard deviation	0.40	3.90	0.49
CV	0.017	0.017	0.022

Appendix 54. Tensile strength of high concentration sol-gel coated fabric C after light exposure to 120 AFU

Replicate	Maximum Load (kgf)	Maximum Load (N)	Tensile extension at Maximum load (mm)
1	21.171	207.6	19.15
2	21.468	210.5	18.85
3	20.897	204.9	18.10
4	20.246	198.5	18.65
5	20.913	205.1	19.40
Mean	20.939	205.3	18.83
Standard deviation	0.45	4.43	0.50
CV	0.021	0.022	0.027